

Galaxy Zoo: disentangling the environmental dependence of morphology and colour[★]

Ramin A. Skibba,^{1†} Steven P. Bamford,^{2,3} Robert C. Nichol,² Chris J. Lintott,⁴ Dan Andreescu,⁵ Edward M. Edmondson,² Phil Murray,⁶ M. Jordan Raddick,⁷ Kevin Schawinski,⁸ Anže Slosar,⁹ Alexander S. Szalay,⁷ Daniel Thomas² and Jan Vandenberg⁷

¹Max-Planck-Institute for Astronomy, Königstuhl 17, D-69117 Heidelberg, Germany

²Institute of Cosmology and Gravitation, University of Portsmouth, Mercantile House, Hampshire Terrace, Portsmouth PO1 2EG

³Centre for Astronomy and Particle Theory, University of Nottingham, University Park, Nottingham NG7 2RD

⁴Astrophysics, University of Oxford, Denys Wilkinson Building, Keble Road, Oxford OX1 3RH

⁵LinkLab, 4506 Graystone Ave., Bronx, NY 10471, USA

⁶Fingerprint Digital Media, 9 Victoria Close, Newtownards, Co. Down, Northern Ireland BT23 7GY

⁷Department of Physics and Astronomy, The Johns Hopkins University, Homewood Campus, Baltimore, MD 21218, USA

⁸Yale Center for Astronomy and Astrophysics, Yale University, PO Box 208121, New Haven, CT 06520, USA

⁹Berkeley Center for Cosmological Physics, Lawrence Berkeley National Lab. & Physics Department, University of California, Berkeley, CA 94720, USA

Accepted 2009 June 29. Received 2009 June 15; in original form 2008 November 20

ABSTRACT

We analyse the environmental dependence of galaxy morphology and colour with two-point clustering statistics, using data from the Galaxy Zoo, the largest sample of visually classified morphologies yet compiled, extracted from the Sloan Digital Sky Survey. We present two-point correlation functions of spiral and early-type galaxies, and we quantify the correlation between morphology and environment with marked correlation functions. These yield clear and precise environmental trends across a wide range of scales, analogous to similar measurements with galaxy colours, indicating that the Galaxy Zoo classifications themselves are very precise. We measure morphology marked correlation functions at fixed colour and find that they are relatively weak, with the only residual correlation being that of red galaxies at small scales, indicating a morphology gradient within haloes for red galaxies. At fixed morphology, we find that the environmental dependence of colour remains strong, and these correlations remain for fixed morphology *and* luminosity. An implication of this is that much of the morphology–density relation is due to the relation between colour and density. Our results also have implications for galaxy evolution: the morphological transformation of galaxies is usually accompanied by a colour transformation, but not necessarily vice versa. A spiral galaxy may move on to the red sequence of the colour–magnitude diagram without quickly becoming an early type. We analyse the significant population of red spiral galaxies, and present evidence that they tend to be located in moderately dense environments and are often satellite galaxies in the outskirts of haloes. Finally, we combine our results to argue that central and satellite galaxies tend to follow different evolutionary paths.

Key words: methods: statistical – galaxies: clusters: general – galaxies: evolution – galaxies: haloes – galaxies: structure – large-scale structure of Universe.

1 INTRODUCTION

The galaxies in the local Universe appear to be classifiable into two broad types: late-type galaxies, with spiral arms, disc-dominated morphologies, ongoing star formation and blue optical colours; and early-type galaxies, with elliptical or bulge-dominated morphologies, old stellar populations and red colours. Many studies have

[★]This publication has been made possible by the participation of more than 100 000 volunteers in the Galaxy Zoo project. Their contributions are individually acknowledged at <http://www.galaxyzoo.org/Volunteers.aspx>

†E-mail: skibba@mpia.de

observed a strong correlation between morphology and environment (i.e. the morphology–density relation), with spiral galaxies tending to be located in low-density environments and elliptical galaxies in more dense environments (e.g. Dressler 1980; Postman & Geller 1984; Norberg et al. 2002; Goto et al. 2003; Blanton et al. 2005; Wolf et al. 2007; Ball, Loveday & Brunner 2008). Other bimodal galaxy properties have also been found to be strongly correlated with the environment: blue galaxies with significant star formation activity tend to reside in underdense environments, while galaxies with red colours and low star formation rates tend to reside in overdense environments (e.g. Lewis et al. 2002; Gómez et al. 2003; Kauffmann et al. 2004; Zehavi et al. 2005; Sheth et al. 2006; Weinmann et al. 2006; Bamford et al. 2008; Tinker et al. 2008; Skibba & Sheth 2009).

In standard Λ cold dark matter (Λ CDM) cosmological models, cold dark matter haloes form from the gravitational collapse of dark matter around peaks in the initial density field. Haloes assemble hierarchically, such that smaller haloes merge to form larger and more massive haloes in dense environments (Mo & White 1996; Sheth & Tormen 2002). According to the current paradigm of galaxy formation, galaxies form within haloes, due to the cooling of hot gas. Halos and galaxies evolve simultaneously, and the evolution of a galaxy is affected by its host halo. If the halo is accreted by a larger halo, the galaxy will be affected by it as well: for example, the galaxy’s diffuse hot gas reservoir may be stripped, removing its fuel for future star formation (e.g. Larson, Tinsley & Caldwell 1980; Balogh, Navarro & Morris 2000; Weinmann et al. 2006; van den Bosch et al. 2008b). Galaxies may also experience major mergers, which transform late-type galaxies into early-type galaxies with a central bulge component (e.g. Driver et al. 2006; Drory & Fisher 2007). Mergers drive gas towards the centre, where it can trigger a burst of star formation and fuel the central black hole, the feedback from which can heat the remaining gas and eventually quench star formation (e.g. Mihos & Hernquist 1996; Wild et al. 2007; Pasquali et al. 2008; Schawinski et al. 2009a).

In this general picture of galaxy formation and evolution, it is expected that galaxies’ morphological and star formation properties are differently correlated with the environment. The purpose of this paper is to shed light on some of these galaxy evolution processes by disentangling the environmental correlations of morphology and colour. We use mark statistics of galaxy clustering, which are sensitive to environmental correlations (e.g. Skibba et al. 2006), with catalogues of galaxies in the Sloan Digital Sky Survey (SDSS; York et al. 2000) to explore the respective roles of morphology and colour in galaxy evolution. We characterize morphologies using classifications from the Galaxy Zoo project (as described in Section 2.2).

This paper is complementary to the work of Bamford et al. (2009), who studied the environmental dependence of morphology and colour with similar catalogues, using projected galaxy density within an adaptive radius and distance to the centre of the nearest galaxy group to characterize the environment. Bamford et al. used these environmental indicators to obtain information about the fractions of galaxy morphologies and colours as an explicit function of environment. However, for their local density estimator, a single density corresponds to a range of scales, while the use of the distance to the nearest group implicitly assumes group-specific environmental mechanisms, in addition to the assumptions of the group-finding algorithm. Our mark clustering statistics yield complementary information, quantifying environmental trends as an explicit function of scale. This paper and Bamford et al. provide very different statistical descriptions of the same data set. In ad-

dition, Bamford et al. explored the environmental dependence of morphology and colour at fixed stellar mass, while we explore the environmental dependence of morphology at fixed colour, and vice versa. Both papers also shed light on the substantial populations of ‘unconventional’ galaxies: red spirals and blue early types. Finally, both the mark correlation functions presented here and the correlations with group mass and luminosity in Bamford et al. can be compared to halo occupation models and semi-analytic models in a straightforward manner.

This paper is organized as follows. In the next section, we describe the Galaxy Zoo data and our volume-limited catalogues. We introduce mark clustering statistics, and in particular, the marked correlation function, in Section 3. In Section 4, we present marked correlation functions using Galaxy Zoo morphology likelihoods as marks, which show the environmental dependence of spiral and early-type morphologies, and of merging and interacting galaxies. Next, we disentangle the environmental dependence of morphology and colour in Section 5, by analysing morphology–environment correlations at fixed colour and colour–environment correlations at fixed morphology. We focus on the populations of red spiral galaxies and blue early-type galaxies in Section 6, and our results allow us to explain their roles in galaxy evolution. Finally, we summarize our results in Section 7.

2 DATA

2.1 Basic catalogue properties

The catalogues used in this paper are constructed from the SDSS Data Release 6 (DR6; Adelman-McCarthy et al. 2008). We consider only the galaxies in the Main Galaxy Sample, extended objects with $r_{\text{petro}} < 17.77$ (Strauss et al. 2002). We also only use galaxies with spectroscopic redshifts.

This raises the issue of fibre collisions, where the thickness of the spectroscopic fibres means that galaxies closer than 55 arcsec on the sky will be missing spectra and redshifts, and hence, absolute magnitudes. This fibre-collision constraint is partly alleviated by the fact that neighbouring plates have overlap regions, but it still results in ~ 7 per cent of targeted galaxies not having a measured redshift. Fibre collisions weakly affect correlation functions at scales of $s \sim 100 \text{ kpc } h^{-1}$ in the redshift space, and mark correlation functions as well, if galaxy spectra are required for accurate marks (Skibba et al. 2006). However, we measure only *projected* marked correlation functions, in which any effects of fibre collisions cancel out (see equation 5). In addition, the fibre assignments were based solely on target positions, and in cases where multiple targets could only have a single fibre assigned, the target selected to be observed was chosen randomly – hence independently of galaxy properties. For the projected correlation functions $w_p(r_p)$, we do not observe any downturn at small scales, which one might expect, due to the higher fraction of missing galaxies. In addition, we have performed tests with similar catalogues with different minimum redshifts, and have also compared some measurements to those of Skibba & Sheth (2009), in which fibre-collided galaxies were included and were given the redshift of their nearest neighbour; in both cases, the correlation functions were consistent at small scales. We conclude that the effects of fibre collisions are negligible for both the projected correlation functions and marked projected correlation functions.

We use Petrosian magnitudes for the galaxy luminosities and colours. Absolute magnitudes are determined using `KCORRECT v4_1_4` (Blanton & Roweis 2007) and are k -corrected and

corrected for passive evolution to $z = 0.1$. We restrict our analysis to volume-limited samples, described in Section 2.3.

Throughout this paper we assume a spatially flat cosmology with $\Omega_m = 0.3$ and $\Omega_\Lambda = 1 - \Omega_m$. We write the Hubble constant as $H_0 = 100 h \text{ km s}^{-1} \text{ Mpc}^{-1}$.

2.2 Galaxy Zoo morphologies

Although galaxy colours are directly measurable, their morphologies are not. A variety of galaxy properties, such as those that quantify the radial light profile of a galaxy, have been used as proxies for galaxy morphologies (e.g. Blanton et al. 2005; van den Bosch et al. 2008a). Automated methods for classifying galaxies using more structural information have also been recently developed (e.g. Conselice 2006; Park et al. 2007). However, none of these techniques can yet provide a direct equivalent of traditional visual morphology. Studies such as Lahav, Naim & Sodr -Lombardi (1996) and Ball et al. (2004) have attempted to reproduce visual morphologies with artificial neural networks. However, their classifications rely heavily on luminosity and colour information, whereas true visual morphology is determined without direct reference to these quantities. The Galaxy Zoo project was born out of a need for reliable, visual morphologies for a large sample of SDSS galaxies. Our approach was to enlist the public’s help to visually classify the morphologies of nearly 1 M galaxies in SDSS DR6 (Adelman-McCarthy et al. 2008). Further details of the Galaxy Zoo project, including its motivation, design and the initial stages of the data reduction, are given in Lintott et al. (2008). We use morphological-type likelihoods estimated from the Galaxy Zoo classifications (Bamford et al. 2009) throughout this paper.

The morphologies utilized here are derived from classifications by over 80 000 members of the international public as part of the Galaxy Zoo project. This project is described in detail by Lintott et al. (2008). Briefly, each galaxy received many, independent morphological classifications, each by a different user. The four possible classifications were labelled as ‘elliptical’, ‘spiral’, ‘do not know’ and ‘merger’. The ‘elliptical’ class, in addition to containing galaxies with elliptical morphology, also contains the majority of S0 galaxies (Bamford et al. 2009). The merger class mainly comprises interacting pairs, generally with tidal features. The spiral classification was subdivided into ‘clockwise’, ‘anticlockwise’ and ‘edge-on/unsure’, referring to the direction and orientation of the spiral arms.

The median number of classifications per object is 34, with 98 per cent of our sample having at least 20 classifications each. These classifications were processed into raw ‘likelihoods’ for a galaxy being of a given morphological type, directly from the proportion of classifications for each type. The raw Galaxy Zoo data set is affected by two redshift-dependent biases. The first is the usual selection bias, due to the apparent magnitude and angular size selection limits of the parent SDSS Main Galaxy Sample. In this paper, we avoid the issue of selection bias by considering only volume-limited samples. The second effect is classification bias: identical galaxies are more likely to be classified as early type with increasing redshift, due to signal-to-noise ratio and resolution effects. Bamford et al. (2009) have quantified the classification bias as a function of galaxy luminosity, size and redshift, which they then use to statistically correct the Galaxy Zoo data. Note that absolutely no reference was made to the environment of the galaxies at any stage of this classification bias correction. Throughout this paper, we utilize the debiased-type likelihoods, which we denote P_{sp} and P_{el} for spiral and early-type likelihoods, respectively.

2.3 Volume-limited catalogues

We perform our analysis on a volume-limited large-scale structure sample. Our catalogue has limits $-23.5 < {}^{0.1}M_r < -19.5$, $0.017 < z < 0.082$, consisting of 99 924 galaxies, with mean number density $\bar{n}_{\text{gal}} = 0.011 (h^{-1} \text{ Mpc})^3$. The superscript of 0.1 refers to the fact that all absolute magnitudes have been k -corrected and evolution-corrected to $z = 0.1$; henceforth, we omit the superscript. This luminosity threshold approximately corresponds to $M_r < M^* + 1$, where M^* is the Schechter function break in the r -band luminosity function (Blanton et al. 2003). It also corresponds to an approximate halo mass threshold of $5.8 \times 10^{11} h^{-1} M_\odot$ (Skibba & Sheth 2009). We have performed the same analysis with a more luminous volume-limited catalogue, with $M_r < -20.5$, and have obtained results qualitatively similar to those presented in Sections 4–6.

There are several ‘false pairs’ of objects in the SDSS – large objects with more than one ID associated with them. This results in extra close pairs being counted. We avoid these objects by calculating their angular separation, and then if the distance is less than either of their Petrosian radii, we exclude the smaller ‘false’ object. There were only a handful of such objects in our volume-limited catalogues.

Most of our analysis is focused on spiral and elliptical galaxies. To avoid ‘contamination’ by other galaxies, we excluded galaxies with high merger or ‘do not know’ likelihoods, with P_{mg} or $P_{\text{dk}} > 15$ per cent or with $P_{\text{sp}} + P_{\text{el}} < 75$ per cent in the measurements, except when stated otherwise. These are conservative cuts, and they reduce the sample size of the catalogues by ~ 10 per cent.

For the measured correlation functions and jack-knife errors, which require random catalogues and jack-knife subcatalogues, we use the hierarchical pixel scheme SDSSPix,¹ which characterizes the survey geometry, including edges and holes from missing fields and areas near bright stars. This same scheme has been used for other clustering analyses (Scranton et al. 2005; Hansen et al. 2009) and for lensing analyses (Sheldon et al. 2007). We use the Scranton et al. jack_random_polygon with window files from SDSS DR5 (Adelman-McCarthy et al. 2007), which reduces the sample size by an additional ~ 20 per cent, to a final size of 72 135 galaxies. For the random catalogues, we used at least 10 times as many random points as in the data, and for each of the error calculations, we used 30 jack-knife subcatalogues. The jack-knife errors of our marked projected correlation functions tend to be larger than the Poisson errors, even at small scales. We note that Norberg et al. (2009) has recently shown that the jack-knife method does not recover the scale dependence of errors of the unmarked correlation function, often overestimating the errors at small scales, and the results are sensitive to the number of subcatalogues into which the data is split. Although our uncertainty estimates are important, our primary results are not particularly sensitive to the precise value of the errors.

3 MARK CLUSTERING STATISTICS AND ENVIRONMENTAL CORRELATIONS

We characterize galaxies by their properties, or ‘marks’, such as their luminosity, colour, morphological type, stellar mass and star formation rate. In most galaxy clustering analyses, a galaxy catalogue is cut into subsamples based on the mark, and the two-point clustering in the subsample is studied by treating each galaxy in

¹ <http://lahmu.phyast.pitt.edu/~scranton/SDSSPix>

it equally (e.g. Norberg et al. 2002; Madgwick et al. 2003; Zehavi et al. 2005; Li et al. 2006; Tinker et al. 2008). These studies have shown that galaxy properties are correlated with the environment, such that elliptical, luminous and redder galaxies tend to be more strongly clustered than spiral, fainter and bluer galaxies. For example, Norberg et al. (2002) divided their catalogue by luminosity and spectral type into subsamples, measured their correlation functions and found that luminous and quiescent galaxies have larger clustering strengths.

However, the galaxy marks in these studies are used to define the subsamples for the analyses, but are not considered further. This procedure is not ideal because the choice of critical threshold for dividing galaxy catalogues is somewhat arbitrary and because throwing away the actual value of the mark represents a loss of information. In the current era of large galaxy surveys, one can now measure not only galaxy clustering as a function of their properties, but the spatial correlations of the galaxy properties themselves. We do this with ‘marked statistics’, in which we weight each galaxy by a particular mark, rather than simply count galaxies as ‘ones’ and ‘zeros’.

Marked clustering statistics have recently been applied to astrophysical data sets by Beisbart & Kerscher (2000), Faltenbacher et al. (2002) and Gottlöber et al. (2002). Marked statistics are well suited for identifying and quantifying correlations between galaxy properties and their environments (Sheth, Connolly & Skibba 2005). They relate traditional unmarked galaxy clustering to the clustering in which each galaxy is weighted by a particular property. Marked statistics are straightforward to measure and interpret: if the weighted and unweighted clustering are significantly different at a particular scale, then the galaxy mark is correlated (or anti-correlated) with the environment at that scale, and the degree to which they are different quantifies the strength of the correlation. In addition, issues that plague traditional clustering measurements, such as incompleteness and complicated survey geometry, do not significantly affect measurements of marked statistics, as these effects cancel out to some extent, since the weighted and unweighted measurements are usually similarly affected. Finally, the halo model framework has been used to interpret the correlations of luminosity and colour marks in terms of the correlation between halo mass and environment (Skibba et al. 2006; Skibba & Sheth 2009). We focus on morphological marks here, and although they could be similarly analysed with the halo model, perhaps by building on these luminosity and colour mark models, that is beyond the scope of this paper.

There are a variety of marked statistics (Beisbart & Kerscher 2000; Sheth 2005), but the easiest to measure and interpret is the marked two-point correlation function. The marked correlation function is simply

$$M(r) \equiv \frac{1 + W(r)}{1 + \xi(r)}, \quad (1)$$

where $\xi(r)$ is the two-point correlation function, the sum over galaxy pairs separated by r , in which all galaxies are ‘weighted’ by unity. $W(r)$ is the same sum over galaxy pairs separated by r , but now each member of the pair is weighted by the ratio of its mark to the mean mark of all the galaxies in the catalogue (e.g. Stoyan & Stoyan 1994). That is, for a given separation r , $\xi(r)$ receives a count of 1 for each galaxy pair, and $W(r)$ receives a count of $W_i W_j$ for $W(r)$. The fact that the marked statistic $M(r)$ can usually be accurately estimated by the simple pair count ratio WW/DD (where DD are the counts of data–data pairs and WW are the weighted counts), without requiring a random galaxy catalogue, implies that

the marked correlation function is less sensitive than the unmarked correlation function to the effects of the survey edges (Sheth et al. 2005). In effect, the denominator in equation (1) divides out the contribution to the weighted correlation function which comes from the spatial contribution of the points, leaving only the contribution from the fluctuations of the marks. That is, the mark correlation function measures the clustering of the marks themselves, in r -scale environments.

In practice, in order to obviate issues involving redshift distortions, we use the projected two-point correlation function

$$w_p(r_p) = \int dr \xi(r_p, \pi) = 2 \int_{r_p}^{\infty} dr \frac{r \xi(r)}{\sqrt{r^2 - r_p^2}}, \quad (2)$$

where $r = \sqrt{r_p^2 + \pi^2}$, r_p and π are the galaxy separations perpendicular and parallel to the line of sight, and we integrate up to line-of-sight separations of $\pi = 40 \text{ Mpc } h^{-1}$. We estimate $\xi(r_p, \pi)$ using the Landy & Szalay (1993) estimator

$$\xi(r_p, \pi) = \frac{DD - 2DR + RR}{RR}, \quad (3)$$

where DD , DR and RR are the normalized counts of data–data, data–random and random–random pairs at each separation bin. Similarly, the weighted projected correlation function is measured by integrating along the line-of-sight the analogous weighted statistic

$$W(r_p, \pi) = \frac{WW - 2WR + RR}{RR}, \quad (4)$$

where W refers to a galaxy weighted by some property (for example, P_{sp} or P_{cl}), and R now refers to an object in the catalogue of random points, weighted by a mark chosen randomly from its distribution. We then define the marked projected correlation function

$$M_p(r_p) = \frac{1 + W_p(r_p)/r_p}{1 + w_p(r_p)/r_p}, \quad (5)$$

which makes $M_p(r_p) \approx M(r)$ on scales larger than a few Mpc. The projected correlation functions w_p and $W_p(r_p)$ are normalized by r_p , so as to be made unitless. On large scales both the real-space and projected marked correlation functions (equations 1 and 5) will approach unity, because at increasing scales the correlation functions $\xi(r)$ and $W(r)$ [or $w_p(r_p)$ and $W_p(r_p)$] become very small as the universe appears nearly homogeneous. The simple ratio of the weighted to the unweighted correlation function $W(r)/\xi(r)$ [or $W_p(r_p)/w_p(r_p)$] approaches unity similarly, provided that there are sufficient number statistics and the catalogue’s volume is sufficiently large.

4 ENVIRONMENTAL DEPENDENCE OF GALAXY MORPHOLOGY

We explore the environmental dependence of galaxy morphology in the Galaxy Zoo in this and the next section by measuring marked projected correlation functions of galaxies in volume-limited catalogues.

When measuring mark clustering statistics, it is important to carefully choose marks that are appropriate for one’s analysis. For example, traditional morphological types of galaxies are discrete marks (e.g. E, S0, Sp and Irr in Norberg et al. 2002; cf. Wolf et al. 2007; Poggianti et al. 2008). Continuous marks can be more useful for analyses of mark correlations, but like discrete marks, they must be measurable with sufficient precision such that contamination by measurement error is not a serious concern. A variety of continuous marks have been used to attempt to characterize the morphological or structural properties of galaxies, such as the Sérsic index,

surface brightness, r_{90}/r_{50} concentration and their combinations (Blanton et al. 2005; Christlein & Zabludoff 2005; Conselice 2006; Park et al. 2007; Scarlata et al. 2007; Ball et al. 2008; van den Bosch et al. 2008a; van der Wel 2008). However, while such structural parameters are no doubt informative, they provide a limited insight concerning the presence of a disc or spiral arms, and are thus not equivalent to traditional visual morphology; rather, they are often more strongly related to galaxy luminosity or colour (see discussion in Bamford et al. 2009).

Here we use the morphological-type *likelihoods* estimated in the Galaxy Zoo (Lintott et al. 2008; see Section 2.2) as marks. The likelihoods were estimated using the visual classifications of the Galaxy Zoo, and are corrected for classification bias (Bamford et al. 2009). These probabilities reflect the certainty with which Galaxy Zoo classifiers were able to assign each galaxy to either of the discrete ‘spiral’ or ‘elliptical’ classes, rather than a continuous measure of morphology. This choice of mark thus encodes our level of knowledge concerning the morphology of each galaxy. The Galaxy Zoo morphologies have been shown to be reliable by comparison with data sets visually classified by professional astronomers. Note that we find that galaxies which are classified as lenticulars by professional astronomers are predominantly placed in the ‘elliptical’ Galaxy Zoo class with high likelihood, and we thus henceforth refer to this class as ‘early type’. As estimates of visual morphology in the standard and generally accepted sense, we believe the Galaxy Zoo classifications to be more suitable for our analysis than the various automatic morphology proxies that have been proposed. The Galaxy Zoo type likelihoods, rather than discrete types or combinations of structural properties, are a reliable choice of mark for exploring the dependence of galaxy morphology on environment.

Mark clustering statistics are sensitive to the distributions of the marks. We begin by presenting morphology mark distributions in Fig. 1, for the $M_r < -19.5$ volume-limited catalogue. The morphology likelihoods P_{sp} and P_{el} are required to be between 0 and 1, and they both are somewhat peaked at the minimum and maximum values, which simply reflects the fact that there is usually good agreement between Galaxy Zoo classifiers on the classification of

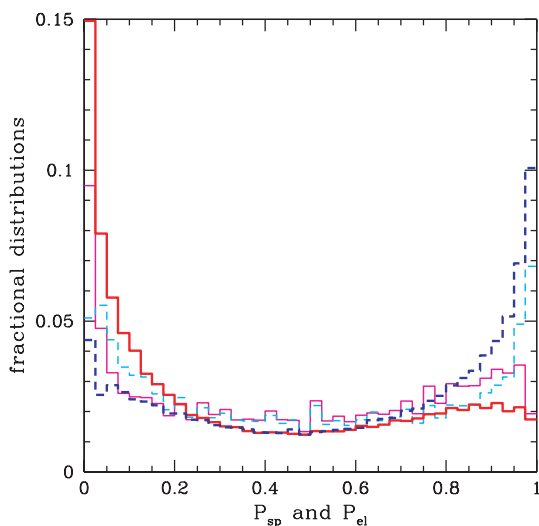


Figure 1. Distributions of morphology marks for $M_r < -19.5$. Thick red (solid) and blue (dashed) histograms show the distributions of P_{el} and P_{sp} , respectively, and thin magenta (solid) and cyan (dashed) histograms show the distributions of their respective uncorrected raw probabilities, prior to the corrections for classification bias.

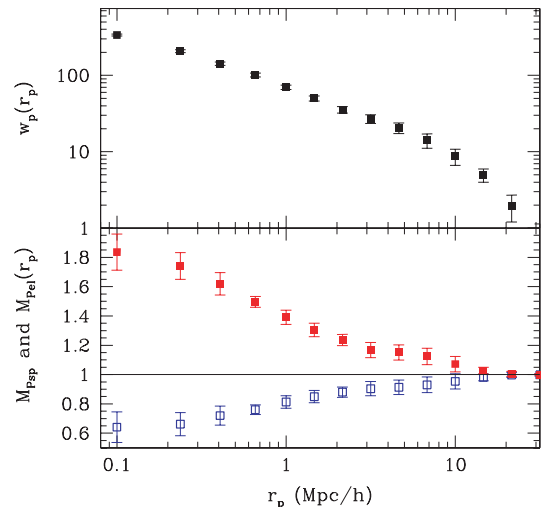


Figure 2. Projected two-point correlation function (upper panel) and mark correlation functions (lower panel) for $M_r < -19.5$. Red (filled) and blue (open) points show the measurements for the P_{el} and P_{sp} marks, with jack-knife error bars.

each object. The figure also clearly shows that the distributions are smoother for the likelihoods corrected for classification bias, discussed in Section 2.2. In what follows, we only use the de-biased type likelihoods for our analysis.

Now we present our morphology mark correlation functions for $M_r < -19.5$ in Fig. 2. At projected separations of $r_p < 10 \text{ Mpc } h^{-1}$, the mark correlations of P_{el} are significantly above unity, indicating that it is correlated with the environment at these scales; that is, early types tend to be located in denser environments. In contrast, the mark correlations of P_{sp} are significantly below unity, indicating that it is anti-correlated with the environment – that is, spirals tend to be located in underdense environments. The scale dependence of the mark correlations is remarkably smooth, monotonically increasing or decreasing towards unity at large scales. The smoothness of these measurements, with no spikes or bumps, is partly due to the large sample size, but it also indicates that the marks have very little noise. This is impressive in itself. Morphological classifications are often very uncertain, but the likelihoods from a large number of classifiers, with robust corrections for ‘classification bias’, appear to be sufficiently precise to yield clear environmental correlations.

The mark correlation functions are a useful tool to show the environmental dependence of morphology, both pairs of galaxies within a single dark matter halo (on small scales, $r_p \leq 2 \text{ Mpc } h^{-1}$), and of pairs in separate haloes (on large scales). In contrast, most other studies of morphology and environment have focused on the surface density within one particular scale (e.g. $1 \text{ Mpc } h^{-1}$) or have used the projected distance or surface density out to the N th nearest neighbour, which mixes different scales together. In Fig. 2, a transition appears to occur in the P_{el} marked correlation function at $r_p \sim 2 \text{ Mpc } h^{-1}$, at the scale of the transition from the ‘one-halo’ to the ‘two-halo’ term. At scales much larger than the size of a typical halo, the scale dependence of marked statistics is simply related to the shape of the linear theory power spectrum (Sheth 2005). The large-scale marked correlation functions are related to morphology-dependent galaxy bias.

The stellar masses of galaxies are correlated with their morphologies and with the environment (e.g. Balogh et al. 2001; Bamford et al. 2009). It is therefore possible that our observed correlation

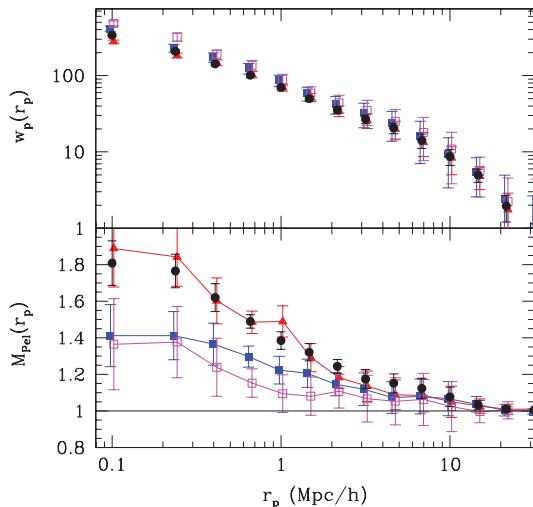


Figure 3. Projected two-point correlation function (upper panel) and P_{el} mark correlation functions (lower panel) for $M_r < -19.5$, for stellar mass intervals: $10.2 \leq \log(M_*/M_\odot) < 10.5$ (triangles), $10.5 \leq \log(M_*/M_\odot) < 10.8$ (filled squares) and $10.8 \leq \log(M_*/M_\odot) < 11.1$ (open squares). Black circles show result for full catalogue (repeated from Fig. 2).

between morphology and environment is simply due to the environmental dependence of stellar mass. In order to test this, we use stellar masses estimated from luminosity and colour, r_{petro} and $(u-r)_{\text{model}}$ (Baldry et al. 2006), and measure the morphology mark correlation functions at fixed stellar mass. The stellar masses have uncertainties of ~ 0.2 dex. We use stellar mass intervals of 0.3 dex: $10.2 \leq \log(M_*/M_\odot) < 10.5$, $10.5 \leq \log(M_*/M_\odot) < 10.8$ and $10.8 \leq \log(M_*/M_\odot) < 11.1$. These subsamples contain 26 037, 22 581 and 9791 galaxies, respectively.

The resulting clustering measurements are shown in Fig. 3. The environmental correlations remain very strong, and for the lowest mass interval, the strength of the correlation is not reduced at all. This is similar to the result obtained by Bamford et al. (2009), that the environmental dependence of the early-type fraction is strong at fixed stellar mass, especially for low-mass galaxies. Even for the most massive galaxies, we find that the environmental correlation is significant out to a few $\text{Mpc } h^{-1}$. The figure shows the result for the P_{el} mark; the result is approximately the same for P_{sp} : the correlation between morphology and environment remains strong even at fixed mass. Therefore, a galaxy of a given stellar mass will be more likely to be an early type (and less likely to be a spiral) in a dense environment compared to a galaxy of the same mass in an underdense environment. Importantly, our stellar masses are estimated from luminosity and colour, both of which are correlated with morphology and the environment (e.g. Blanton et al. 2005; Park et al. 2007). In addition, the environmental dependence of stellar mass, as characterized by mark correlations, can be entirely described by the combined environmental dependence of luminosity and colour (Skibba & Sheth, in preparation). It has long been known that the morphologies and colours of galaxies are closely related (e.g. Hubble 1936; de Vaucouleurs 1961; Strateva et al. 2001), and we attempt to disentangle the environmental correlations of these properties in Section 5.

For all of these mark correlation measurements, in order to focus on the population of galaxies most likely to be spirals or early types, we have excluded galaxies with P_{mg} or $P_{\text{dk}} > 15$ per cent or with $P_{\text{sp}} + P_{\text{el}} < 75$ per cent. Consequently, for nearly all galaxies in the catalogue, the sum of P_{sp} and P_{el} is nearly unity (i.e. $1 - P_{\text{sp}}$ is

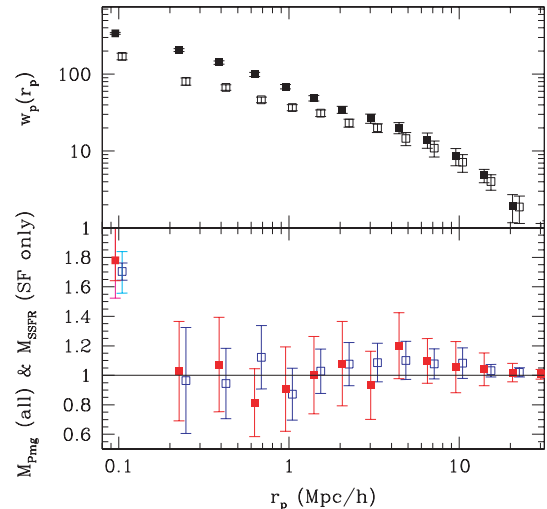


Figure 4. Projected two-point correlation function and P_{mg} mark correlation function for all galaxies in the $M_r < -19.5$ catalogue (filled square points). For comparison, measurement from Skibba, Wake & Sheth (in preparation) of $w_p(r_p)$ and $\text{SFR}/M_* M(r_p)$ of star-forming galaxies is also shown (open square points). For $M(r_p)$ at $100 \text{ kpc } h^{-1}$, error bars show 1σ and 2σ of the distributions of measurements from jack-knife sampling.

almost equivalent to P_{el}). If these cuts were not made, however, the mark correlations using the $1 - P_{\text{sp}}$ mark is slightly weaker than those of P_{el} , indicating that P_{mg} , or even P_{dk} , is weakly correlated with the environment.

We show the measurement of the P_{mg} mark correlation function in Fig. 4, now with no cuts on the morphological-type likelihoods. P_{mg} quantifies the likelihood with which a galaxy is classified as undergoing an interaction or merger, usually with indications of tidal distortions or tails; heavily distorted objects may be more likely to be classified with a high P_{dk} ('do not know'). The P_{mg} likelihoods are generally quite accurate, such that every galaxy in the Galaxy Zoo with $P_{\text{mg}} \geq 0.6$ has been found to show clear evidence of merging (Darg et al. 2009a). The probability that a galaxy is observed to be undergoing a merger or interaction is approximately uncorrelated with the environment except at scales of $r_p \sim 100 \text{ kpc } h^{-1}$, where it spikes upwards at $M(r_p) = 1.78^{+0.42}_{-0.25}$. (This point has a wide bin width of galaxy separations, $1.75 < \log(r_p/\text{kpc } h^{-1}) < 2.25$, though we obtain a similar spike when we repeat the measurement using a narrower bin and when we vary only the lower or upper limit of the bin.) We have also measured the marked correlation function on even smaller scales, and $M(r_p)$ appears to rise to ≈ 3 at $r_p = 50 \text{ kpc } h^{-1}$ and ≈ 30 at $r_p = 25 \text{ kpc } h^{-1}$, though such measurements are very uncertain.

Interestingly, this is very similar to the mark correlation function of the Brinchmann et al. (2004) specific star formation rate (SFR/M_*) mark measured by Skibba, Wake & Sheth (in preparation), for a similar $M_r < -19.5$ volume-limited catalogue (open points in Fig. 4). Their measurement is for highly star-forming galaxies *only*, with strong emission lines ($\text{H}\alpha$, $\text{H}\beta$, $[\text{O III}]$, $[\text{N II}]$, with AGN excluded), which is why there is no large-scale trend. The extinction-corrected SFR ($\text{H}\alpha$) mark correlation function also displays similar behaviour. This result is consistent with the picture that mergers, and interactions between galaxies can drive gas into their central regions, triggering bursts of star formation. In a thorough investigation of merging and interacting galaxies in the Galaxy Zoo, Darg et al. (2009a) have similarly found that the specific SFRs

are about twice as high in star-forming merging galaxies than in star-forming control galaxies. Our result is also consistent with Robaina et al. (2009), who find a similar small-scale enhancement of star formation at $z \sim 0.6$, also using visually classified morphologies, with SFRs estimated from ultraviolet (UV) and infrared (IR) luminosity.

The correlation between P_{mg} and the environment is not unexpected: mergers and interactions are relatively common in groups and clusters, and rare in underdense environments. It is interesting that the mark correlations are significant out to $r_p \approx 170 \text{ kpc } h^{-1}$ (the maximum separation for the bin centred on $r_p = 100 \text{ kpc } h^{-1}$), which is near the virial radius of the minimum halo mass associated with the luminosity threshold of the galaxy catalogue, estimated from halo occupation modelling (see Skibba & Sheth 2009). This suggests that much of the signal is due to galaxy pairs interacting and influencing each other in the central regions of dark matter haloes with masses above this threshold. However, this scale should be interpreted with caution, because the effects of galaxy mergers and interactions on morphologies and star formation are expected to be important on much smaller scales ($r < 40 \text{ kpc}$). Our measurements do not imply that these effects persist out to larger scales: for example, two galaxies i and j with a separation $170 \text{ kpc } h^{-1}$ and a relatively large mark product $P_{\text{mg},i} P_{\text{mg},j}$ might not be merging with each other. Rather, they may both be located in a small-scale environment in which the occurrence of mergers is relatively likely. The scale of the upturn in the mark correlation function has a simple physical explanation: mergers tend to occupy slightly denser environments than average, often in galaxy groups (McIntosh et al. 2008; Darg et al. 2009b). Galaxy pairs in groups are often found at projected separations of $r_p < 200 \text{ kpc } h^{-1}$, and some of them may have recently experienced a merger or interaction. Galaxy mergers also occur in clusters, where galaxies often have larger projected separations, but the fraction of galaxies that are merging is relatively low.

We also note that our result in Fig. 4, although suggestive, does not imply a *necessary* connection between the processes of merging and star formation: the merging/interacting and starbursting galaxy pairs are not necessarily the same, and even if they are, we cannot by these methods establish a causal connection. Because the mark distributions are so different and because of the uncertainties involved, we cannot draw stronger conclusions at this time.

Note that the Galaxy Zoo merger/interaction likelihoods have other potential uses as well. For example, they could be used to estimate merger rates or fractions, as has been done with other morphological classifications (e.g. de Propris et al. 2007; Lotz et al. 2008). Galaxy close pair counts have been used extensively for this purpose, but P_{mg} *weighted* pair counts could also contribute to such studies, or could be used as tests for other methods. We can define the following as the fraction of galaxies within a distance r_f that show signs of merging (e.g. distortions or tidal tails that indicate a significant gravitational interaction):

$$f_{\text{merg}}(r < r_f) = \frac{4\pi\bar{n}_{\text{gal}} \langle P_{\text{mg}} \rangle^2 \int_0^{r_f} dr r^2 [1 + W_{P_{\text{mg}}}(r)]}{4\pi\bar{n}_{\text{gal}} \int_0^{r_f} dr r^2 [1 + \xi(r)]}, \quad (6)$$

where the denominator is the close pair fraction, (see Bell et al. 2006; Masjedi et al. 2006) and $W_{P_{\text{mg}}}(r)$ is the *real-space* P_{mg} weighted correlation function, normalized by the mean mark $\langle P_{\text{mg}} \rangle$ (which is approximately 0.027 for the catalogue used for Fig. 4) squared. If the real-space weighted and unweighted correlations can be reliably estimated at small scales, then this fraction can be estimated as well. However, our measured P_{mg} weighted correlation function is very

uncertain at such small scales, and robustly estimating the value of f_{merg} is beyond the scope of this paper.

Finally, Slosar et al. (2009) have detected a chiral correlation function in the spins of spiral galaxies at small galaxy separations. Using tidal torque theory, they interpret this result as correlated angular momenta. However, it is also plausible that spiral arms could be enhanced or even induced by galaxy–galaxy interactions in a manner that is consistent with their signal. This could be tested with a mark cross-correlation function, to determine whether spiral chirality and disturbed morphology are correlated at small scales. In a related issue, Jimenez et al. (2009) recently found a correlation between past star formation activity and the degree of coherence of spin direction, especially for galaxies that formed most of their stars in the past. The fact that nearby spiral galaxies may have similar star formation histories and aligned spins is interpreted as the result of the large-scale environment influencing both halo spins and star formation activity.

5 DISENTANGLING MORPHOLOGY AND COLOUR

The previous section showed the environmental dependence of galaxy morphology using mark correlation functions with the Galaxy Zoo. It is well known, however, that morphology and colour are strongly correlated (e.g. Blanton et al. 2005; Ball et al. 2008; van der Wel 2008), and that galaxy colour is also correlated with the environment (e.g. Zehavi et al. 2005; Berlind et al. 2006; Wang et al. 2008; Coil et al. 2008; Cooper et al. 2008; Tinker et al. 2008; Bamford et al. 2009; Skibba & Sheth 2009; cf. Weinmann et al. 2006; Skibba 2009 for the different correlations of central and satellite galaxies). As galaxies evolve, their star formation properties and structural properties are expected to transform differently (van den Bosch et al. 2008a); therefore, if we can disentangle the dependence of morphology and colour on the environment, we can shed some light on aspects of galaxy evolution. The main purpose of this section is to separate the environmental dependence of morphology and colour, and we do this by analysing morphology mark correlation functions at fixed colour and colour mark correlation functions at fixed morphology.

5.1 Environmental dependence of morphology at fixed colour

We begin by explicitly showing the correlation between the Galaxy Zoo likelihoods P_{el} and P_{sp} , and $g - r$ colour, in Fig. 5. The correlation is strongest for likelihoods between 0.3 and 0.7, and in the colour range $0.8 < g - r < 0.95$. Note also that there is significant scatter across the whole range in colour and morphology likelihood, but especially at the red end of the plot. We have also measured the morphology *fractions* as a function of colour (see Bamford et al. 2009), which also indicate that, while most blue galaxies are spirals, a significant fraction of red galaxies are not early types.

In Fig. 6, we show the projected clustering of all galaxies, and of red and blue galaxies separately, using the following colour–magnitude cut (used by Blanton & Berlind 2007; Skibba & Sheth 2009):

$$(g - r)_{\text{cut}} = 0.8 - 0.03(M_r + 20). \quad (7)$$

Note that this is different from the $u - r$ versus M_r colour–magnitude cut used by Bamford et al. (2009); we do not expect our results to be sensitive to the exact choice of the cut.

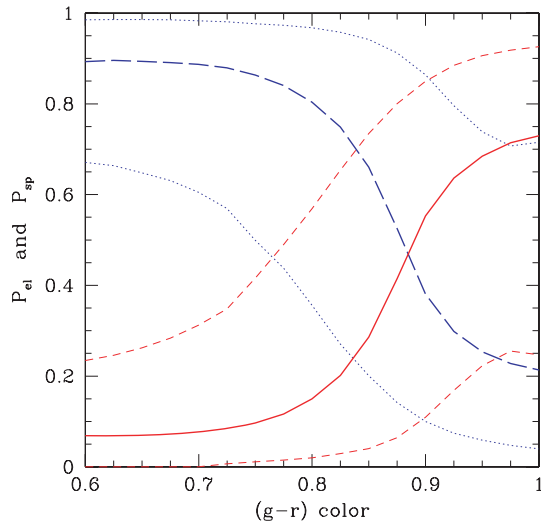


Figure 5. Median correlation between P_{el} likelihood and $g-r$ colour (red solid curve), and P_{sp} and $g-r$ (blue long-dashed curve) in the $M_r < -19.5$ volume-limited catalogue. Thin lines show the 16 and 84 percentiles.

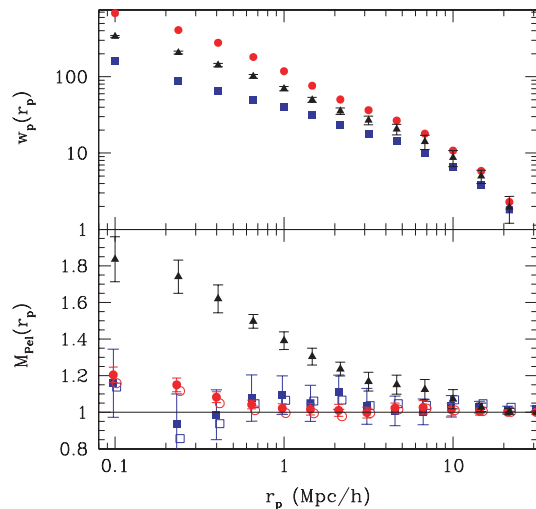


Figure 6. Projected correlation function (upper panel) and P_{el} mark correlation function (lower panel) of all galaxies in the $M_r < -19.5$ catalogue (black triangles, from Fig. 2) compared to that of red and blue galaxies (red circle points and blue square points, respectively). ‘Red’ and ‘blue’ galaxy subcatalogues are determined using the colour–magnitude cut in equation (7) (filled points) or using the colour likelihood thresholds $P_{red} > 0.8$ and $P_{blu} > 0.8$ (open points).

The upper panel of the figure simply shows that red galaxies are more strongly clustered than blue galaxies. The lower panel shows the environmental dependence of morphology at fixed colour. In particular, we compare the P_{el} mark correlation function for all galaxies (from Fig. 2) to the P_{el} mark correlation functions for red and blue galaxies (circle and square points). The morphology mark signal is considerably weakened at fixed colour.

Therefore, the correlations between morphology and environment are extremely weak at fixed colour: blue galaxies have no morphology–environment correlation, and for red galaxies, only a weak residual correlation at small scales remains. This implies that much of the correlation between morphology and environment is explained by that of colour and environment, and the remaining

environmental dependence occurs only on scales smaller than the diameter of a typical dark matter halo.

Colour gradients or ‘segregation’ within haloes, defined with respect to the halo radii, have been observed in group and cluster catalogues (Hansen et al. 2009; van den Bosch et al. 2008b), and they appear to be approximately independent of halo mass. [Note that colour gradients are much stronger than luminosity gradients (Hansen et al. 2009); since galaxy stellar masses are well described by their luminosities and colours (Bell et al. 2003), this suggests that, at least for some subpopulations of galaxies, the environmental dependence of their stellar populations is such that the observed stellar mass segregation within groups (van den Bosch et al. 2008b) manifests itself observationally merely as colour segregation.] Such gradients as a function of halo-centric or group-centric distance result in slightly stronger mark correlations, but only at small scales (Skibba 2009). The fact that the residual correlation in Fig. 6 occurs only at scales of $r_p < 500 \text{ kpc } h^{-1}$, that is, predominantly within dark matter haloes, suggests that in haloes of a given mass, red early types are more strongly clustered than the whole red galaxy population. It is possible that this correlation is related to stellar mass segregation in haloes, because although Bamford et al. (2009) observe a similar small-scale morphology–environment correlation at fixed stellar mass, it is relatively weak. However, if the morphology gradient were mostly due to stellar mass segregation, then at fixed stellar mass, most of the morphology–environment correlation should disappear at small scales, but this is clearly not the case (see lower panel of Fig. 3).

In any case, we interpret the residual mark correlation in Fig. 6 such that haloes may host both red early types (red galaxies with high P_{el}) and red spirals (red galaxies with low P_{el}), but the latter tend to be located further from the halo centre and are more likely to be ‘satellite’ galaxies. The galaxy pairs at small separations consist mostly of central–satellite pairs, and therefore red satellites closer to a red central galaxy in a given halo are more likely to be early types than red satellites further away. If there were a significant halo mass dependence of morphology at fixed colour, then the marked correlations would have to be statistically significant [i.e. inconsistent with $M(r_p) = 1$] on larger scales – scales at which the clustering statistics are dominated by the contribution from pairs in separate haloes – but we do not observe such a correlation in Fig. 6. In the halo model, massive dark matter haloes are more strongly clustered than less massive haloes (e.g. Mo & White 1996); when large-scale galaxy clustering depends on a galaxy property, indicated by significant large-scale marked correlations, this implies that the property, at least for central galaxies, is correlated with halo mass (Sheth 2005; Skibba et al. 2006; Skibba & Sheth 2009), but this is not the case here for morphology at fixed colour.

It follows from this argument that galaxy morphologies depend more on colour and halo-centric distance than on halo mass, so at fixed (red) colours, we expect a morphology gradient within haloes. For example, we expect that $P_{morph}(r/r_{vir}|g-r, M_{halo})$ is not constant for galaxies with red $g-r$, which is a prediction that can be tested with satellite galaxies in group catalogues. We have also observed a somewhat similar P_{el} correlation for red galaxies in a more luminous catalogue, and hence for galaxies in more massive haloes, so it is possible that the strength of this gradient is approximately independent of halo mass (for haloes with $M_{halo} > 6 \times 10^{11} M_{\odot} h^{-1}$), but our results are not conclusive on this point. If this is the case, then it would imply that the transformation of red spiral satellite galaxies into red lenticular and elliptical galaxies occurs similarly in all environments. On the other hand, if the transformation mechanisms that change these galaxies’ morphologies, such

as ram-pressure stripping, galaxy merging and tidal ‘harassment’, depend on halo mass, then they may be more (or less) efficient in more massive haloes, resulting in a different morphology gradient in haloes of different mass.

We have also performed similar measurements with a stricter colour–magnitude cut, using colour *likelihoods*, analogous to the morphology likelihoods. In particular, we use the bimodal $g - r$ colour distribution as a function of r -band luminosity: the red sequence and its rms, the blue sequence and its rms, and the blue fraction, as a function of luminosity (Skibba & Sheth 2009). With this information, we estimate each galaxy’s P_{red} and P_{blu} (normalized to total unity) based on its position on the $(g - r) - M_r$ colour–magnitude diagram. When we use the stricter cuts of $P_{\text{red}} > 0.8$ and $P_{\text{blu}} > 0.8$ (open points in Fig. 6), the result is the same: at fixed colour, there is almost no morphology–environment correlation. This complements the result from Bamford et al. (2009), who found that at fixed stellar mass (determined from $u - r$ colour and r -band luminosity), there is only a weak residual correlation between early-type fraction and projected density and almost no correlation between early-type fraction and projected distance to the nearest galaxy group (their figs 11 and 14).

Note that the distributions of morphology likelihoods are different for red and blue galaxies. Since mark clustering statistics are sensitive to the distributions of the marks, it is possible that the weakening of the environmental correlations in Fig. 6 is simply due to differences between the distributions. However, we show in the appendix that, even after accounting for the different mark distributions, the correlation between morphology and environment at fixed colour is still relatively weak.

5.2 Environmental dependence of colour at fixed morphology

We now perform a similar analysis of the environmental dependence of galaxy colour at fixed morphology. In Fig. 7, we show the projected clustering of all galaxies, and of early-type and spiral galaxies separately. The upper panel simply shows that early-type

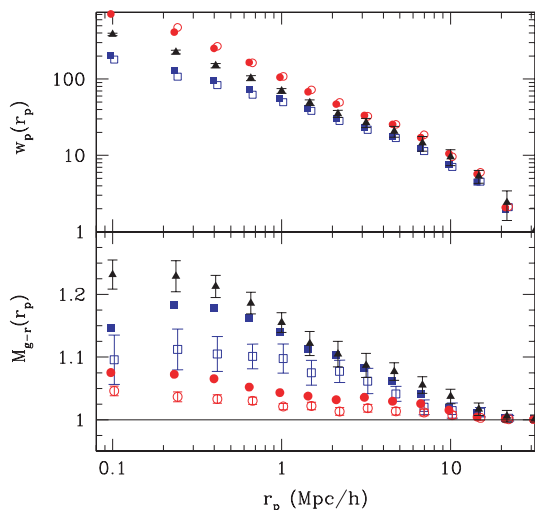


Figure 7. Projected correlation function (upper panel) and $g - r$ colour mark correlation function (lower panel) of all galaxies in the $M_r < -19.5$ catalogue from Skibba & Sheth (2009) (triangle points) compared to that of early-type and spiral galaxies (red circle points and blue square points, respectively). The spiral and early-type subcatalogues are determined using the greater morphology likelihood as the distinguishing criterion (filled points) or using the likelihood threshold of $P > 0.8$ (open points).

galaxies are more strongly clustered than spirals. The lower panel shows the environmental dependence of colour at fixed morphology, analogous to Fig. 6 in Section 5.1. In particular, we compare the $g - r$ colour mark correlation function of all galaxies (from Skibba & Sheth 2009) to that of early types and spirals. The lower values of $M(r_p)$ here compared to Fig. 6 are simply due to the different distributions of colour and morphology likelihoods. The galaxy colours are always within a factor of 1.5 of the mean colour, while the morphology likelihoods vary by more than an order of magnitude. Therefore, the mark product of the colours of a galaxy pair in a dense environment may not be that much larger than the mark product of a pair in an underdense environment, while the difference between the pairs’ morphology likelihood marks may be much larger.

If one simply counts spiral galaxies as those with $P_{\text{sp}} > P_{\text{el}}$, and early types as the rest, then the resulting colour mark correlations are somewhat weakened (solid square points), but are still very significant out to large scales ($r_p \sim 10 \text{ Mpc } h^{-1}$). If one applies stricter thresholds, with $P_{\text{sp}} > 0.8$ for spirals and $P_{\text{el}} > 0.8$ for early types, then the mark correlations are weakened slightly further (open square points), but they remain significant out to large scales. This result is robust, and it is not affected by the different colour distributions of spirals and early types (Appendix A). The fact that we see strong mark correlations out to large-scale separations in Fig. 7, in contrast to Fig. 6, implies that at fixed morphology, galaxy colours are correlated with the environment: at a given morphology likelihood, galaxies tend to be redder in more massive systems (e.g. clusters) than in less massive systems (e.g. groups).

We have also measured colour mark correlation functions at fixed morphology and luminosity, and have found significant residual environmental trends. For example, in Fig. 8, we show the $g - r$ mark correlation function of spiral galaxies (with $P_{\text{sp}} > 0.8$) in luminosity bins of $-20 < M_r < -19.5$, $-20.5 < M_r < -20$ and $-21 < M_r < -20.5$. The uncertainties are large because the subsamples are small, consisting of 11 216, 9022 and 5621 galaxies, respectively. For the two fainter bins, we detect a statistically significant marked signal out to large scales ($r_p \approx 8 \text{ Mpc } h^{-1}$), while the measurement of the third luminosity bin is consistent with no trend. We have obtained a

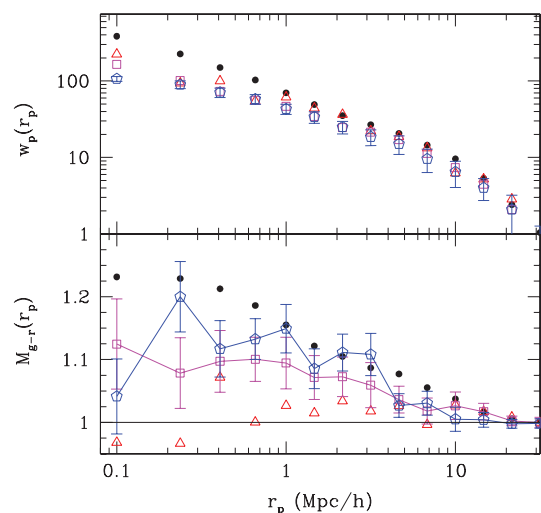


Figure 8. Projected correlation functions and $g - r$ mark correlation functions, as in Fig. 7, but for spiral galaxies ($P_{\text{sp}} > 0.8$) in three luminosity bins: $-20 < M_r < -19.5$ (blue pentagons), $-20.5 < M_r < -20$ (magenta squares) and $-21 < M_r < -20.5$ (red triangles). Error bars are shown only for the fainter two subsamples, and the points are connected, for clarity.

similar result for early-type galaxies, with significant environmental correlations for fainter galaxies and a very weak trend for $-21 < M_r < -20.5$. These results are consistent with those of Bamford et al. (2009): at faint luminosities, the colours of both spirals and early types are correlated with the environment, while at bright luminosities, most galaxies of any morphology are fairly red, and the narrow colour distribution results in weaker or non-existent colour mark correlations. This also explains the weak colour–environment correlation observed by Schawinski et al. (2007), whose sample of early types is brighter and smaller than ours.

Therefore, *at fixed morphology and luminosity, a relatively strong correlation between colour and environment remains.* This is in stark contrast to the result in the previous section, that at fixed colour, almost no morphology–environment correlation remains. The results in Figs 6 and 7 show that the morphology–density relation is to a significant extent a colour–density relation, which is consistent with the results from other studies (Blanton et al. 2005; Quintero et al. 2006; Wolf et al. 2007; Bamford et al. 2009). Contrary to these studies and the results in this paper, Park et al. (2007) claim that the key galaxy property is morphology, and that at fixed morphology and luminosity, galaxy colour is nearly independent of the environment. Their disagreement may be due to the fact that their morphology classification was explicitly based on galaxy colours and colour gradients, while we, Bamford et al. and Wolf et al. used visual classifications, and Blanton et al. and Quintero et al. used the Sérsic index and surface brightness as morphological indicators.

It is worth noting that, as pointed out by Quintero et al. (2006), it is possible in principle that the strong colour–environment correlation and extremely weak morphology–environment correlation are due to the measurement errors of the marks. In particular, it is possible that (i) the errors of the morphology likelihoods are much larger than those of the colours, and in an extreme case, so large that they wash out some of the environmental correlations and (ii) the errors themselves could be correlated with each other and with the environment. However, first, our error analyses show that the uncertainties in the morphology mark correlation functions are only slightly larger than those of the colour mark correlation functions. Secondly, the Galaxy Zoo morphology classifications were done independently of the environment and were tested with black and white images (Lintott et al. 2008). The corrections for classification bias (Bamford et al. 2009) also appear to be robust for the redshifts to which our volume-limited catalogue is restricted. We conclude that the errors of the morphologies and colours can have only a minimal impact on our correlation function measurements, and they do not affect our results.

The results in this section have implications for galaxy evolution. They suggest first that a morphology transformation is usually accompanied by a colour transformation: that is, if a galaxy transforms from a spiral to an early type, its star formation is quenched and it becomes red on a relatively short time-scale. On the other hand, a colour transformation can occur without a morphological transformation: for example, a spiral galaxy can move on to the red sequence without becoming an early type. Such ‘red spirals’ are the subject of Section 6.

5.3 Combined environmental dependence of morphology and colour

Finally, we compare the relative strength of the environmental correlations of colour and morphology in Fig. 9. In order to compare more directly to the morphology likelihoods, instead of using the colours of galaxies, we now use their colour likelihoods (described

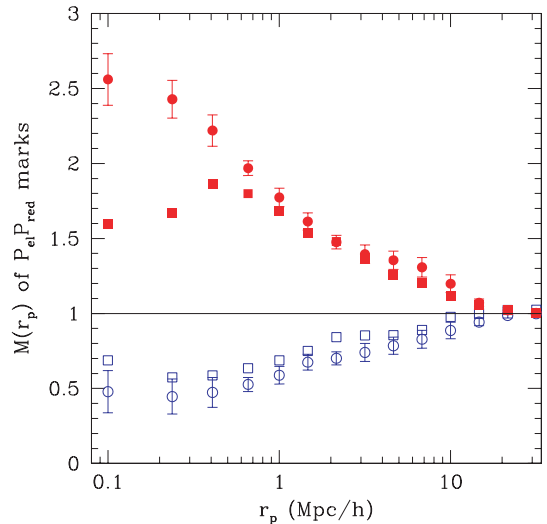


Figure 9. Morphology–colour mark correlation functions, for the following marks: $P_{el}P_{red}$ (red filled circles), $P_{sp}P_{red}$ (red filled squares), $P_{el}P_{blu}$ (blue open squares) and $P_{sp}P_{blu}$ (blue open circles).

earlier in this section), estimated from the $(g - r) - M_r$ colour distribution as a function of luminosity. Like the colour likelihoods, we now also normalize P_{el} and P_{sp} by $P_{el} + P_{sp}$ here, so that they also total unity. The P_{el} and P_{red} mark distributions, and their effect on the mark correlations, are discussed in Appendix A.

Fig. 9 shows the result, where we mark each galaxy by the four morphology–colour combinations of P_{el} and P_{sp} , and P_{red} and P_{blu} . First, by comparing the red and blue circle points to the red and blue points in Fig. 2, the environmental correlations for the $P_{el}P_{red}$ and $P_{sp}P_{blu}$ marks are clearly magnified, due to the combined environmental dependence of both morphology and colour. That is, red early types tend to be located in very dense environments, while blue spirals tend to reside in very underdense environments. In addition, on scales of $r_p < 500 \text{ kpc } h^{-1}$, the environmental dependence of the red early types appears to be stronger than the environmental anticorrelations of the blue spirals: for example, $M_{P_{red}P_{el}}(r_p)$ (red circles) rises to ≈ 2.5 at $r_p \approx 100 \text{ kpc } h^{-1}$ (i.e. the weighted correlation function is 2.5 times stronger than the unweighted correlation function), while $M_{P_{blu}P_{sp}}(r_p)$ drops only to ≈ 0.5 (i.e. the weighted correlation function is only twice weaker than the unweighted correlation function). This may be an indication that the vast majority of red early types are central galaxies.

Secondly, for the $P_{sp}P_{red}$ and $P_{el}P_{blu}$ marks, one might expect that the mark signal would be weak or non-existent, as these are combining opposite environmental correlations. None the less, the mark correlations are fairly strong and significant out to large scales, and their direction suggests that environmental dependence of colour is stronger than that of morphology. In principle, this could be due to the fact the P_{red} distribution is different from P_{el} (which is equivalent to $1 - P_{sp}$ here). However, even after accounting for the different distributions (in the appendix), we still find that galaxies with high P_{red} and P_{sp} tend to reside in denser environments than average, where the environment is measured in the range $100 \text{ kpc } h^{-1} < r_p < 10 \text{ Mpc } h^{-1}$.

There is a downturn in the measurement for the $P_{sp}P_{red}$ mark at small scales ($r_p < 300 \text{ kpc } h^{-1}$), which may be due to the relatively high satellite fraction of red spirals (discussed in the next section), resulting in a suppressed central-satellite term, and also may be partly due to morphology gradients within haloes, if they

are stronger than colour gradients (i.e. if P_{sp} decreases more rapidly than P_{red} increases at small halo-centric radii). The behaviour of the mark correlation function also demonstrates that the morphology likelihoods and colour likelihoods contain independent information, and that the former is not derivative of the latter.

In any case, the main conclusion from Fig. 9 is that redder, more spiral structured galaxies tend to be located in denser environments than average, and red early types are even more strongly correlated with the environment.

6 RED SPIRAL GALAXIES

While red early-type galaxies and blue late-type galaxies are abundant and well known, we now turn to the less understood population of red spiral galaxies. We simply define red spirals as all those galaxies redder than the colour–magnitude cut (7) and with $P_{\text{sp}} > 0.8$. We showed in Section 5 that at fixed colour the morphology–environment correlation is relatively weak, while at fixed morphology some of the colour–environment correlation remains. It follows from this that a morphology transformation of a galaxy usually implies a concomitant colour transformation, so galaxies that transform into early types while remaining blue should be rare. In contrast, some galaxies that move on to the red sequence may not undergo a morphology transformation, so there should be a significant population of red spiral galaxies. For our $M_r < -19.5$ volume-limited catalogue, after excluding galaxies with high likelihoods of P_{mg} or P_{dk} , 8443 galaxies out of 90 400 are red spirals (9.3 per cent), while only 654 are blue early types (0.7 per cent). Since red spiral galaxies are relatively common, while blue early types are not, we focus this section on the red spirals. Schawinski et al. (2009b) have investigated in detail the blue early types in the Galaxy Zoo.

It is worth noting that Schiminovich et al. (2007) found, using UV–optical colours and a dust correction based on 4000 Å break strength and spectral energy distribution (SED) fits, that passive disc-dominated galaxies are relatively rare. It is therefore possible that a significant fraction of the red spirals in our sample have some ongoing star formation, but are reddened by dust extinction. Semi-analytic models also show significant dust extinction among disc-dominated galaxies, with the dust optical depth having a strong correlation with gas mass and anticorrelation with scale radius (Fontanot et al. 2009). Using a combination of IR and UV/optical data, Gallazzi et al. (2009) and Wolf et al. (2009) find in the outskirts of the A901/902 supercluster a significant population of red, yet star-forming, spirals, with relatively high masses and low Sérsic indices. These objects appear red due to low SFRs and their residual star formation being highly extinguished, and are particularly prevalent at intermediate densities. We will argue that a large fraction of the red spiral galaxies in the Galaxy Zoo are indeed satellite galaxies; their emission line statistics are currently being investigated.

Fig. 2 showed that spiral galaxies tend to reside in underdense environments, or low-mass dark matter haloes, while Fig. 7 showed that red galaxies tend to reside in overdense environments, or massive haloes. We focus now on the galaxies that are both red and spiral. We compare the correlation function of red spiral galaxies to those of all red galaxies and all spiral galaxies in Fig. 10. The clustering of red spirals is consistent with that of red galaxies at large scales. However, at small scales ($r_p < 2 \text{ Mpc } h^{-1}$), on the scales of galaxy pairs within the same halo, their clustering signal is significantly depressed. This result is consistent with Bamford et al. (2009), who found that the fraction of red spirals, and of red face-on

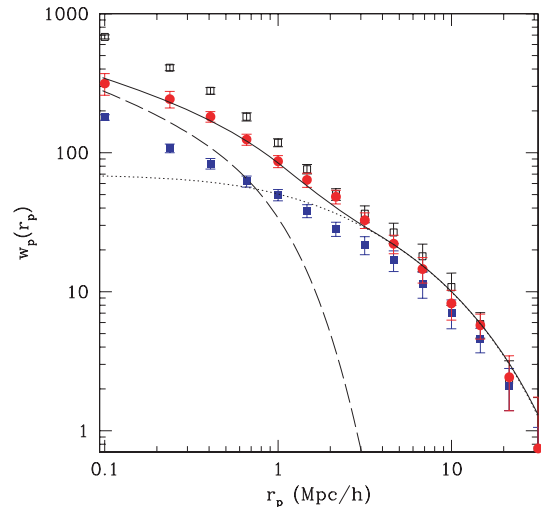


Figure 10. Projected two-point correlation function of red spiral galaxies (red circles) compared to that of all red galaxies (black open squares) and that of all spiral galaxies (blue filled squares) in the $M_r < -19.5$ catalogue. A halo occupation model of the correlation function is also shown (solid curve), consisting of galaxy pairs in a single halo (dashed curve) and in separate haloes (dotted curve). The model is consistent with the measurement, with $\chi^2_{\text{d.o.f.}} = 0.5$.

spirals alone, increases with projected galaxy density, except in the densest environments (i.e. in cluster cores), in which the fraction drops.

This suggests that red spirals are often satellite galaxies in the outskirts of groups and clusters, while red early types tend to be located in the inner regions of these groups. This is consistent with our interpretation of the weak residual morphology–environment correlation of red galaxies in Fig. 6.

We test this with a halo occupation model of galaxy clustering (e.g. Zehavi et al. 2005; Zheng, Coil & Zehavi 2007) in which the halo occupation distribution of central and satellite galaxies depends on halo mass and the luminosity threshold. In Fig. 10, we show the result of such a model, using mean halo occupation functions described in appendix A2 of Skibba & Sheth (2008). In simple halo occupation models, for galaxies more luminous than some threshold ($M_r < -19.5$ in this case), corresponding to an approximate halo mass threshold ($M_{\text{min}} \approx 5.8 \times 10^{11} h^{-1} M_{\odot}$), haloes are occupied by a single central galaxy and N_{sat} satellite galaxies, where $\langle N_{\text{sat}} | M, L_{\text{min}} \rangle \approx (M/M_1)^{\alpha}$, $M_1 \propto M_{\text{min}}(L_{\text{min}})$ and α increases with L_{min} . In practice, we account for the fact that there is significant scatter in the relation between central galaxy luminosity and halo mass, and that the satellite halo occupation function drops off more rapidly than a power law at low masses just above M_{min} . The satellite galaxy fraction is then

$$f_{\text{sat}} = \frac{\int_{M_{\text{min}}} dM (dn/dM) \langle N_{\text{sat}} | M, L_{\text{min}} \rangle}{\int_{M_{\text{min}}} dM (dn/dM) (\langle N_{\text{cen}} | M \rangle + \langle N_{\text{sat}} | M, L_{\text{min}} \rangle)}, \quad (8)$$

where dn/dM is the halo mass function. The range of models that approximately fit the measurement (with $\chi^2_{\text{d.o.f.}} < 1$) have a satellite fraction of $f_{\text{sat}} \approx 32$ per cent. This is 50 per cent larger than the satellite fraction of all galaxies with $M_r < -19.5$, $f_{\text{sat}} \approx 24$ per cent.

There are two significant differences between the models that fit the correlation function of red spirals in the figure and the fiducial model for all galaxies brighter than the luminosity threshold. First, and most importantly, the halo mass threshold M_{min} for red spirals is

about 0.1–0.2 dex larger than that of the whole population, while the parameter M_1 , which characterizes the amplitude of the mean halo occupation function and approximately corresponds to the mass of a halo that hosts one satellite on average, is only ≈ 12 times larger than M_{\min} , rather than the fiducial factor of ≈ 20 . The slope α of the halo occupation function is unchanged. If instead α were much larger for red spirals, indicating more galaxies in more massive haloes, and M_1/M_{\min} were unchanged, then red spirals would be predominantly located in massive, cluster-sized haloes. However, such models are ruled out by the measurement. Since M_1/M_{\min} has a lower value, the mean of the halo occupation distribution $\langle N_{\text{sat}} \rangle$ is relatively large even in lower mass haloes, indicating that the red spiral satellite galaxies are expected to reside in haloes with a wide range in mass. Although red spirals have been observed in the outskirts of galaxy clusters (hosted by high-mass haloes, with $M > 10^{14} h^{-1} M_{\odot}$), we predict that they are located in galaxy groups as well (hosted by less massive haloes, with masses as low as $10^{13} h^{-1} M_{\odot}$). Secondly, in order to fit the suppressed correlation function at scales of $r_p < 500 \text{ kpc } h^{-1}$, models in which the satellite galaxy number density profile is less concentrated (by a factor of 3) than the dark matter profile are favoured. However, this parameter is not well constrained.

We now address the possibility that our results are affected by dust reddening and galaxy inclinations. For example, a significant fraction of edge-on SOs could be mistakenly classified as spirals, or star-forming edge-on spirals could be sufficiently dusty to satisfy our colour criterion for ‘red spirals’. Corrections for inclination-related effects are available in the literature (Masters, Giovanelli & Haynes 2003; Shao et al. 2007; Maller et al. 2009), and they are not negligible. In the Galaxy Zoo, we can determine whether objects were classified as spiral due to the presence of visible spiral arms or simply due to a discy, edge-on appearance. Following Bamford et al. (2009), we define as ‘edge-on/unclear’ those objects for which the majority of classifiers could not individually discern a spiral arm direction ($p_{\text{CW}} + p_{\text{ACW}} < p_{\text{EU}}$, where CW, ACW and EU refer to clockwise, anticlockwise and edge-on/unclear, respectively). Note that this is conservative, as even if a minority of classifiers can discern spiral arms in a galaxy, then it is very likely to be a spiral.

In Fig. 11, we compare the clustering of red edge-on spirals (galaxies redder than the colour cut in equation 7, with $p_{\text{CW}} + p_{\text{ACW}} < p_{\text{EU}}$ and with $P_{\text{sp}} > 0.8$) and of red face-on spirals (redder than the colour cut, with $p_{\text{CW}} + p_{\text{ACW}} > p_{\text{EU}}$ and with $P_{\text{sp}} > 0.8$). The red edge-on spirals outnumber the red face-on ones by a factor of more than 3:1. The red edge-on spirals appear slightly less strongly clustered than the red face-on spirals, consistent with the hypothesis that many of them are star-forming galaxies, which tend to be located in underdense environments. None the less, the difference between the clustering measurements is of very weak statistical significance. We have also used the apparent axis ratio (b/a) as an observational inclination indicator, and have found that, for red spiral galaxies, it too does not depend strongly on the environment. In addition, the b/a distributions of red spirals and blue spirals are similar, especially when the spiral arms are visible. These tests show that galaxy inclinations can have only a minimal effect on our results, and they do not affect our conclusions. A detailed investigation of the effects of dust and inclination on spiral galaxies in the Galaxy Zoo is currently underway.

Finally, we show the colour–magnitude diagram of red spiral galaxies compared to that of all red galaxies and all spiral galaxies in Fig. 12. Red spirals consist of 18 per cent of the total population of red galaxies and also 23 per cent of the spiral galaxy population.

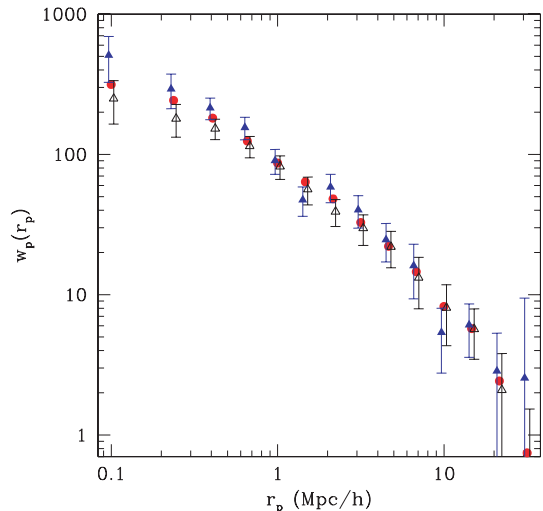


Figure 11. Projected correlation function of red edge-on spirals (open triangles), red face-on spirals (filled triangles) and all red spiral galaxies (red circles, same as Fig. 10) in the $M_r < -19.5$ catalogue. The points have been slightly offset in $\log r_p$, for clarity.

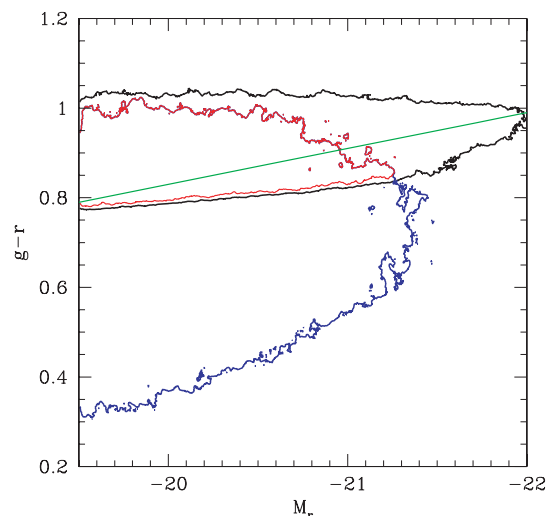


Figure 12. $(g - r) - M_r$ colour–magnitude diagram for the $M_r < -19.5$ catalogue. Red contour circumscribes most of the red spiral galaxies; black and blue contours circumscribe most of the red galaxies and spiral galaxies, respectively. The contours encompass colour–magnitude points with galaxy counts that are 5 per cent or more of the maximum count in the *full* catalogue (which is peaked at $g - r = 0.92$, $M_r = -19.9$), thus showing the relative contribution of each subset of the data. The satellite galaxy mean colour–magnitude sequence of Skibba & Sheth (2009) is also shown (green line).

Perhaps not surprisingly, red spirals are concentrated at the fainter, somewhat bluer part of the red sequence. The majority of spiral galaxies occupy the ‘blue cloud’, although they have a wide range in colour at fixed luminosity.

We interpreted the clustering result in Fig. 10, and in particular the suppressed small-scale correlation function of red spiral galaxies, as evidence that red spirals are often satellite galaxies. In the colour–magnitude diagram in Fig. 12, we have also plotted the satellite galaxy mean colour–magnitude sequence of Skibba & Sheth (2009) and Skibba (2009), which they found to be consistent with measurements of colour mark correlation functions in

the SDSS, and with the satellite colours as a function of luminosity and group richness in SDSS group catalogues. Skibba (2009) showed that a large fraction of faint satellites are somewhat blue, and argued that many are likely still undergoing processes of star formation quenching, while the majority of brighter satellites tend to lie on the red sequence.

The fact that the satellite galaxy colour sequence in the figure goes through the colour–magnitude region occupied by blue spirals at faint luminosities ($M_r \geq -19.5$), red spirals at intermediate luminosities ($-21 \leq M_r \leq -19.5$) and red early types at bright luminosities ($M_r < -21$) suggests that satellites tend to follow a particular evolutionary sequence. First, it suggests that the time-scale of the morphological transformation of these galaxies is longer than that of the quenching of their star formation, consistent with the analysis of Wolf et al. (2009). Secondly, it is useful to recall that while faint satellites can be found in dark matter haloes of all masses, bright satellites tend to reside only in massive haloes (Skibba, Sheth & Martino 2007). Therefore, while red spiral satellite galaxies may be potentially found in haloes of a wide range in mass, red early-type satellites are rarer and tend to be found only in massive haloes, in the inner regions of galaxy clusters. Consequently, we argue that many red spirals are satellites in groups and clusters, in a variety of environments, and were formally blue spirals whose star formation has been suppressed. This picture is consistent with the analysis of van den Bosch et al. (2008a).

In contrast, central galaxies have a bluer mean colour sequence as a function of luminosity than satellites. At a given luminosity, central galaxies tend to be slightly bluer than satellites and tend to be in less massive haloes, although central galaxies account for the vast majority of luminous red galaxies, in more massive haloes (Skibba 2009). We interpret the strong correlation between colour and environment for spiral galaxies (Fig. 7) such that most blue spirals are central galaxies in low-mass haloes (i.e. in less dense environments), while red spirals are either central galaxies in intermediate-mass haloes (with masses up to $M \sim 10^{13} h^{-1} M_\odot$, corresponding to $M_r \sim -21$) or satellites in more massive haloes (with masses $M \geq 10^{13} h^{-1} M_\odot$, i.e. in denser environments). The red spiral central galaxies tend to be located in galaxy groups, because of the correlation between halo mass and group richness. Following mergers with their own satellites, these central galaxies could form bulges with supermassive black holes, and transform their morphologies into lenticular and elliptical types (the GZ early-type class). If these groups are accreted on to clusters, the former central galaxies would be the origin of the red early-type satellites in massive haloes. This picture is consistent with the analysis of Bell (2008), Pasquali et al. (2009), Schawinski et al. (2009a) and Schiminovich et al. (2007).

The different relations between morphology and colour and between morphology and group mass for central and satellite galaxies are currently being investigated further (Skibba et al., in preparation), with the galaxy group catalogue of Yang et al. (2007).

7 DISCUSSION

We have used volume-limited galaxy catalogues from the SDSS Data Release 6 (Adelman-McCarthy et al. 2008) with data from the Galaxy Zoo (Lintott et al. 2008) to study the environmental dependence of galaxy morphology and colour. The Galaxy Zoo project produced a large catalogue of visual morphological galaxy classifications, yielding reliable morphological-type likelihoods for hundreds of thousands of galaxies. We measured projected two-point correlation functions and marked correlation functions, and we used the latter to identify and quantify the environmental cor-

relations of morphological-type likelihoods and $g - r$ colour on a wide range of scales.

We summarize our results as follows.

(i) We measured marked correlation functions using the marks P_{sp} and P_{et} , the likelihoods of a galaxy being a spiral and early type, respectively. These showed clear environmental trends such that at all scales probed, spiral galaxies tend to reside in less dense environments and early-type galaxies tend to be located in overdense environments. Furthermore, the scale dependence of the mark correlations is remarkably smooth, indicating that the marks have very little noise – that is, the Galaxy Zoo morphological-type likelihoods, which have been corrected for classification bias, are very precise.

(ii) We also measured the P_{mg} (merger/interaction likelihood) marked correlation function, and found that it is strongly correlated with the environment at scales up to $r_p \approx 170 \text{ kpc } h^{-1}$. That is, galaxies on these scales have a much larger likelihood of showing evidence of mergers and interactions than average. We compared this measurement to a specific SFR marked correlation function measured with a catalogue with similar volume limits (Skibba et al., in preparation), and showed that it too is strongly peaked at the same scale and is uncorrelated with the environment at larger scales. Naturally, merging and interacting galaxies are normally studied at very small scales, at separations of $r_p < 40 \text{ kpc } h^{-1}$, which is closer than we can reliably probe. However, our result shows either that the effects of galaxy interactions and bursts of star formation persist out to separations of $r_p \approx 170 \text{ kpc } h^{-1}$ or more, or that for galaxies with neighbours on these scales, a significant fraction of their neighbours are merging and star bursting. While we cannot conclusively claim that there is a causal connection between mergers and star formation, our result is consistent with the picture that mergers and interactions between galaxies trigger star formation in them.

Studies that attempt to identify both galaxies in interacting systems frequently miss interacting objects, due to selection criteria and difficulties in determining line-of-sight separations, for example. Measuring the mark correlation function, using the merging/interacting *likelihood* as the mark, provides a complementary way of assessing the frequency and properties of galaxy interactions, effective to larger separations, and including all interacting objects, in a statistical sense.

(iii) We have sought to disentangle the environmental dependence of morphology and colour by measuring morphology marked correlation functions at fixed colour and colour marked correlation functions at fixed morphology. We found that blue galaxies show no correlation between morphology and environment at all scales, and red galaxies are weakly correlated with the environment at small scales only ($r_p < 500 \text{ kpc } h^{-1}$). The fact that this correlation occurs in the ‘one-halo term’, at separations smaller than the size of massive dark matter haloes, is interpreted as an indication of morphology gradients within haloes: red galaxies in the outer regions of haloes tend to be spirals while those in the inner regions tend to be early types. Because of the correlation between galaxy colours and mass-to-light ratios (e.g. Baldry et al. 2006), this also implies a morphology gradient for massive galaxies.

(iv) In contrast, at fixed morphology, a relatively strong correlation between colour and environment remains. In particular, both spiral and early-type galaxies show significant colour–environment correlations out to scales of $r_p \sim 10 \text{ Mpc } h^{-1}$, and the colours of the latter have the stronger environmental dependence (see Fig. A4). That is, red spiral galaxies tend to be located in denser environments than blue spirals, and red early types tend to be located in the densest environments, at any scale the environment is measured.

The fact that the morphology–environment correlation is very weak at fixed colour while the colour–environment correlation remains strong at fixed morphology implies that the morphology–density relation could be more accurately viewed as a colour–density relation, which is consistent with the conclusions of other studies (Blanton et al. 2005; Wolf et al. 2007; Bamford et al. 2009).

(v) We used the bimodal $g - r$ colour distribution as a function of r -band luminosity (Skibba & Sheth 2009) to estimate colour likelihoods of galaxies, P_{red} and P_{blu} , analogous to the morphology likelihoods P_{el} and P_{sp} . We used these four likelihoods together as marks, and found that the marked correlation function with the P_{sp} P_{red} mark is significantly above unity. That is, the opposite environmental correlations did not cancel out; instead, the environmental dependence of colour is much stronger than that of morphology.

(vi) This result shows that galaxies that are both red and spiral tend to be located in dense environments. These red spiral galaxies are not insignificant: they are 9 per cent of the galaxies in the $M_r < -19.5$ volume-limited catalogue, and they account for nearly a quarter of all the spirals. We compared the correlation function of red spiral galaxies to that of all red galaxies and of spirals, and found that the clustering of red spirals is similar to that of red galaxies on large scales, but is depressed on scales of $r_p < 2 \text{ Mpc } h^{-1}$, in the one-halo term, indicating that they have a high satellite fraction. This is more evidence that many red spiral galaxies are satellite galaxies. Skibba & Sheth (2009) and Skibba (2009) showed that satellite galaxies tend to follow a particular sequence on the colour–magnitude diagram, and it passes through the region of the diagram occupied by red spirals. These results suggest that satellite galaxies evolve a particular way: faint satellites are accreted as blue late types, and then they experience ‘strangulation’, in which their hot gas reservoirs are stripped, causing their star formation to be gradually suppressed while they retain spiral morphology.

ACKNOWLEDGMENTS

We thank Aday Robaina, Anna Gallazzi, Frank van den Bosch, Ravi Sheth and David Hogg for valuable discussions about our results. We also thank the anonymous referee for a careful reading of the paper and for helpful suggestions that improved it.

We thank Jeffrey Gardner, Andrew Connolly and Cameron McBride for assistance with their *Ntropy* code, which was used to measure all of the correlation functions presented here. *Ntropy* was funded by the NASA Advanced Information Systems Research Program grant NNG05GA60G.

This work has depended on the participation of many members of the public in visually classifying SDSS galaxies on the Galaxy Zoo web site. We thank them for their extraordinary efforts in making this project a success. We are also indebted to various members of the media, both traditional and online, for helping to bring this project to the public attention.

Funding for the SDSS and SDSS-II has been provided by the Alfred P. Sloan Foundation, the Participating Institutions, the National Science Foundation, the US Department of Energy, the National Aeronautics and Space Administration, the Japanese Monbukagakusho, the Max Planck Society and the Higher Education Funding Council for England. The SDSS web site is <http://www.sdss.org/>.

The SDSS is managed by the Astrophysical Research Consortium for the Participating Institutions. The Participating Institutions are the American Museum of Natural History, Astrophysical Institute Potsdam, University of Basel, Cambridge University, Case Western Reserve University, University of Chicago, Drexel

University, Fermilab, the Institute for Advanced Study, the Japan Participation Group, Johns Hopkins University, the Joint Institute for Nuclear Astrophysics, the Kavli Institute for Particle Astrophysics and Cosmology, the Korean Scientist Group, the Chinese Academy of Sciences (LAMOST), Los Alamos National Laboratory, the Max-Planck-Institute for Astronomy (MPA), the Max-Planck-Institute for Astrophysics (MPIA), New Mexico State University, Ohio State University, University of Pittsburgh, University of Portsmouth, Princeton University, the United States Naval Observatory and the University of Washington.

REFERENCES

- Adelman-McCarthy J. K. et al., 2007, *ApJS*, 172, 634
 Adelman-McCarthy J. K. et al., 2008, *ApJS*, 175, 297
 Baldry I. K., Balogh M. L., Bower R. G., Glazebrook K., Nichol R. C., Bamford S. P., Budavari T., 2006, *MNRAS*, 373, 469
 Ball N. M., Loveday J., Fukugita M., Nakamura O., Okamura S., Brinkmann J., Brunner R. J., 2004, *MNRAS*, 348, 1038
 Ball N. M., Loveday J., Brunner R. J., 2008, *MNRAS*, 383, 907
 Balogh M. L., Navarro J. F., Morris S. L., 2000, *ApJ*, 540, 113
 Balogh M. L., Christlein D., Zabludoff A. I., Zaritsky D., 2001, *ApJ*, 557, 117
 Bamford S. P., Rojas A. L., Nichol R. C., Miller C. J., Wasserman L., Genovese C. R., Freeman P. E., 2008, *MNRAS*, 391, 607
 Bamford S. P. et al., 2009, *MNRAS*, 393, 1324
 Beisbart C., Kerscher M., 2000, *ApJ*, 545, 6
 Bell E. F., 2008, *ApJ*, 682, 355
 Bell E. F., McIntosh D. H., Katz N., Weinberg M. D., 2003, *ApJS*, 149, 289
 Bell E. F., Phleps S., Somerville R. S., Wolf C., Borch A., Meisenheimer K., 2006, *ApJ*, 652, 270
 Berlind A. A., Kazin E., Blanton M. R., Pueblas S., Scoccimarro R., Hogg D. W., 2006, *ApJ*, submitted (astro-ph/0610524)
 Blanton M. R., Berlind A. A., 2007, *ApJ*, 664, 791
 Blanton M. R., Roweis S., 2007, *AJ*, 133, 734
 Blanton M. R., Eisenstein D., Hogg D. W., Schlegel D. J., Brinkmann J., 2005, *ApJ*, 629, 143
 Brinchmann J., Charlot S., White S. D. M., Tremonti C., Kauffmann G., Heckman T., Brinkmann J., 2004, *MNRAS*, 351, 1151
 Christlein D., Zabludoff A. I., 2005, *ApJ*, 621, 201
 Coil A. L. et al., 2008, *ApJ*, 672, 153
 Conselice C. J., 2006, *MNRAS*, 373, 1389
 Cooper M. C. et al., 2008, *MNRAS*, 383, 1058
 Darg D. et al., 2009a, *MNRAS*, submitted (arXiv:0903.4937)
 Darg D. et al., 2009b, *MNRAS*, submitted (arXiv:0903.5057)
 de Propris R. et al., 2007, *ApJ*, 666, 212
 de Vaucouleurs G., 1961, *ApJS*, 5, 233
 Dressler A., 1980, *ApJ*, 236, 351
 Driver S. P. et al., 2006, *MNRAS*, 368, 414
 Drory N., Fisher D. B., 2007, *ApJ*, 664, 640
 Faltenbacher A., Gottlöber S., Kerscher M., Müller V., 2002, *A&A*, 395, 1
 Fontanot F., Somerville R. S., Silva L., Monaco P., Skibba R., 2009, *MNRAS*, 392, 553
 Gallazzi A. et al., 2009, *ApJ*, 690, 1883
 Gómez P. L. et al., 2003, *ApJ*, 584, 210
 Goto T., Yamauchi C., Fujita Y., Okamura S., Sekiguchi M., Smail I., Bernardi M., Gomez P. L., 2003, *MNRAS*, 346, 601
 Gottlöber S., Kerscher M., Kravtsov A. V., Faltenbacher A., Klypin A., Müller V., 2002, *A&A*, 387, 778
 Hansen S. M., Sheldon E. S., Wechsler R. H., Koester B. P., 2009, *ApJ*, 699, 1333
 Hubble E. P., 1936, *Realm of the Nebulae*. Yale Univ. Press, New Haven
 Jimenez R. et al., 2009, preprint (arXiv:0906.0994)
 Kauffmann G., White S. D. M., Heckman T. M., Ménard B., Brinchmann J., Charlot S., Tremonti C., Brinkmann J., 2004, *MNRAS*, 353, 713
 Lahav O., Naim A., Sodré-Lombardi M. C., 1996, *MNRAS*, 283, 207

Landy S. D., Szalay A. S., 1993, *ApJ*, 412, 64
 Larson R. B., Tinsley B. M., Caldwell C. N., 1980, *ApJ*, 237, L692
 Lewis I. et al., 2002, *MNRAS*, 334, L673
 Li C., Kauffmann G., Jing Y. P., White S. D. M., Börner G., Cheng F. Z., 2006, *MNRAS*, 368, 21
 Lintott C. J. et al., 2008, *MNRAS*, 389, 1179
 Lotz J. M. et al., 2008, *ApJ*, 672, 177
 McIntosh D. H., Guo Y., Hertzberg J., Katz N., Mo H. J., van den Bosch F. C., Yang X., 2008, *MNRAS*, 388, 1537
 Madgwick D. S. et al., 2003, *MNRAS*, 344, 847
 Maller A. H., Berlind A. A., Blanton M. R., Hogg D. W., 2009, *ApJ*, 691, 394
 Masjedi M. et al., 2006, *ApJ*, 644, 54
 Masters K. L., Giovanelli R., Haynes M. P., 2003, *AJ*, 126, 158
 Mihos J. C., Hernquist L., 1996, *ApJ*, 464, 641
 Mo H. J., White S. D. M., 1996, *MNRAS*, 282, 347
 Norberg P. et al., 2002, *MNRAS*, 332, 827
 Norberg P., Baugh C. M., Gaztañaga E., Croton D. J., 2009, *MNRAS*, 396, 19
 Park C., Choi Y.-Y., Vogeley M. S., Gott J. R., III, Blanton M. R., 2007, *ApJ*, 658, 898
 Pasquali A., van den Bosch F. C., Mo H. J., Yang X., Somerville R., 2009, *MNRAS*, 394, 38
 Poggianti B. M. et al., 2008, *ApJ*, 684, 888
 Postman M., Geller M. J., 1984, *ApJ*, 281, 95
 Quintero A. D., Berlind A. A., Blanton M. R., Hogg D. W., 2006, preprint (astro-ph/0611361)
 Robaina A. R. et al., 2009, *ApJ*, submitted (arXiv:0907.3728)
 Scarlata C. et al., 2007, *ApJS*, 172, 406
 Schawinski K. et al., 2007, *ApJS*, 173, 512
 Schawinski K. et al., 2009a, *ApJ*, 690, 1672
 Schawinski K. et al., 2009b, *MNRAS*, 396, 818
 Schiminovich D. et al., 2007, *ApJ*, 173, 315
 Scranton R. et al., 2005, *ApJ*, 633, 589
 Shao Z., Xiao Q., Shen S., Mo H. J., Xia X., Deng Z., 2007, *ApJ*, 659, 1159
 Sheth R. K., 2005, *MNRAS*, 364, 796
 Sheth R. K., Tormen G., 2002, *MNRAS*, 329, 61
 Sheth R. K., Connolly A. J., Skibba R., 2005, preprint (astro-ph/0511773)
 Sheth R. K., Jimenez R., Panter B., Heavens A. F., 2006, *ApJ*, 650, L25
 Skibba R. A., 2009, *MNRAS*, 392, 1467
 Skibba R. A., Sheth R. K., 2009, *MNRAS*, 392, 1080
 Skibba R. A., Sheth R. K., Connolly A. J., Scranton R., 2006, *MNRAS*, 369, 68
 Skibba R. A., Sheth R. K., Martino M. C., 2007, *MNRAS*, 382, 1940
 Slosar A. et al., 2009, *MNRAS*, 392, 1225
 Stoyan D., Stoyan H., 1994, *Fractals, Random Shapes, and Point Fields*. Wiley, Chichester
 Strateva I. et al., 2001, *AJ*, 122, 1861
 Strauss M. A. et al., 2002, *AJ*, 124, 1810
 Tinker J. L., Conroy C., Norberg P., Patiri S. G., Weinberg D. H., Warren M. S., 2008, *ApJ*, 686, 53
 van den Bosch F. C., Aquino D., Yang X., Mo H. J., Pasquali A., McIntosh D. H., Weinmann S. M., Kang X., 2008a, *MNRAS*, 387, 79
 van den Bosch F. C., Pasquali A., Yang X., Mo H. J., Weinmann S., McIntosh D. H., Aquino D., 2008b, preprint (arXiv:0805.0002)
 van der Wel A., 2008, *ApJ*, 675, L13
 Wang Y., Yang X., Mo H. J., van den Bosch F. C., Weinmann S. M., Chu Y., 2008, *ApJ*, 687, 919
 Weinmann S. M., van den Bosch F. C., Yang X., Mo H. J., 2006, *MNRAS*, 366, 2
 Wild V., Kauffmann G., Heckman T., Charlot S., Lemson G., Brinchmann J., Reichard T., Pasquali A., 2007, *MNRAS*, 381, 543
 Wolf C., Gray M. E., Aragón-Salamanca A., Lane K. P., Meisenheimer K., 2007, *MNRAS*, 376, L1
 Wolf C. et al., 2009, *MNRAS*, 393, 1302
 Yang X., Mo H. J., van den Bosch F. C., Pasquali A., Li C., Barden M., 2007, *ApJ*, 671, 153
 York D. G. et al., 2000, *AJ*, 120, 1579

Zehavi I. et al., 2005, *ApJ*, 630, 1
 Zheng Z., Coil A. L., Zehavi I., 2007, *ApJ*, 667, 760

APPENDIX A: MARK DISTRIBUTIONS AND THEIR EFFECT ON THE MARKED CORRELATION FUNCTIONS

Mark correlation functions are sensitive to the distributions of the marks. In this appendix, we show the mark distributions for the measurements in Section 5, in which we compared the environmental dependence of galaxy morphology and colour, and we show how the mark correlation measurements are affected when one accounts for the different mark distributions.

In Fig. A1, we show the distribution of P_{el} morphology likelihood (normalized by $P_{el} + P_{sp}$), for red and blue galaxies, where ‘red’ and ‘blue’ refers to the colour likelihoods estimated from the $g - r$ colour distribution as a function of r -band luminosity (Skibba & Sheth 2009), for $P_{red} > 0.8$ and $P_{blu} > 0.8$. Not surprisingly, a larger fraction of red galaxies than blue galaxies are early types, and a larger fraction of blue galaxies are spirals.

In order to account for the different mark distributions for the mark correlation functions of red and blue galaxies, we rescale their P_{el} mark distributions, so that they have the same distribution as that of all galaxies (black histogram in Fig. A1). The procedure is simple: if there are N marks in a catalogue, then we generate N random marks such that they have the required distribution. Then we sort these marks and replace the original marks in the catalogue with them. We maintain the rank order of the galaxies’ marks; only their distribution has changed.

Following this procedure, we repeated the measurements in Fig. 6 with the rescaled marks for red and blue galaxies. The result is shown in Fig. A2, and it is almost exactly the same. The morphology gradient of red galaxies on small scales is slightly stronger. There is a hint of a positive environmental correlation for blue galaxies, which could be interpreted as an indication that blue early types tend to reside in denser environments than blue spirals, but this trend is of weak significance (only $\sim 1\sigma$).

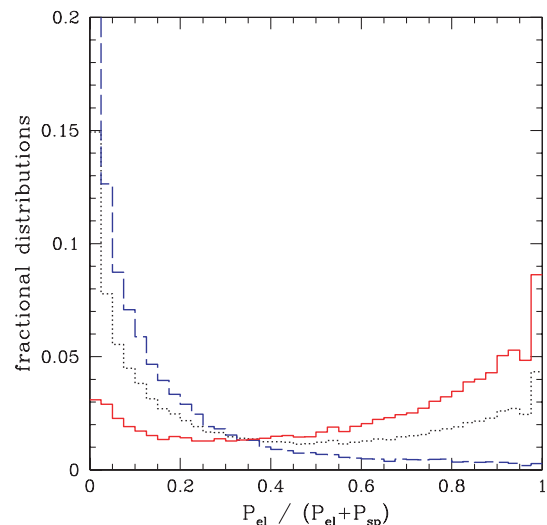


Figure A1. $P_{el}/(P_{el} + P_{sp})$ distributions of all galaxies (black dotted histogram), red galaxies (red solid histogram) and blue galaxies (blue dashed histogram), with $P_{red} > 0.8$ and $P_{blu} > 0.8$, in the $M_r < -19.5$ volume-limited catalogue.

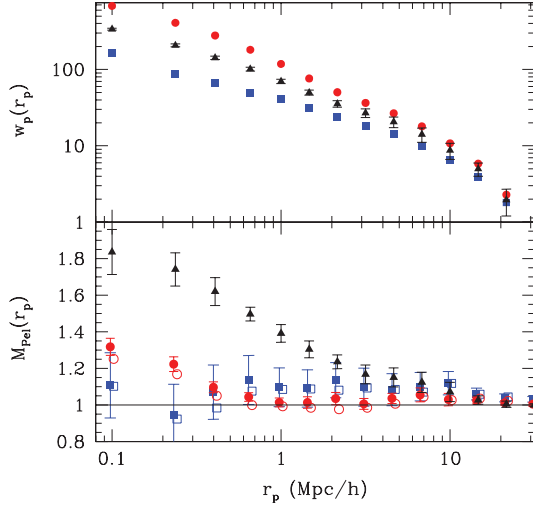


Figure A2. P_{el} marked correlation function (lower panel) of all galaxies in the $M_r < -19.5$ catalogue (black triangles) compared to that of red and blue galaxies (red circle points and blue square points), as in Fig. 6, but with the mark distributions forced to match the black dotted histogram in Fig. A1. ‘Red’ and ‘blue’ galaxy subcatalogues are determined using the colour–magnitude cut in equation (7) (filled points) or using the colour likelihood thresholds $P_{\text{red}} > 0.8$ and $P_{\text{blu}} > 0.8$ (open points). The positions of the galaxies are unchanged, so the unmarked correlation functions (upper panel) are the same as before.

Next, we show the distribution of $g - r$ colour for spiral and early-type galaxies, with $P_{\text{sp}} > 0.8$ and $P_{\text{el}} > 0.8$, in Fig. A3. The distribution for early types is strongly peaked on the red sequence, while spirals have a wide and smooth distribution, with a significant red fraction.

We now rescale the colour mark distributions, with the same procedure as before, forcing the spiral and early-type subsamples to have the same colour distribution as that of all galaxies (black dotted histogram in Fig. A3). The resulting colour marked correlation functions are shown in Fig. A4. This result clearly shows that red

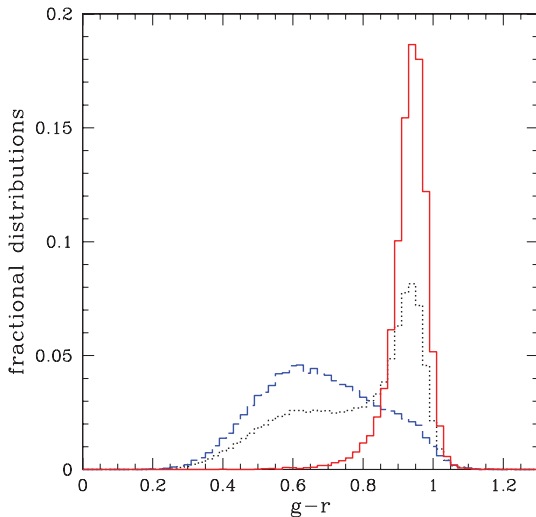


Figure A3. $g - r$ colour distributions of all galaxies (black dotted histogram), early-type galaxies (red solid histogram) and spiral galaxies (blue dashed histogram), in the $M_r < -19.5$ volume-limited catalogue. Spiral and early-type galaxies are defined with $P_{\text{sp}} > 0.8$ and $P_{\text{el}} > 0.8$, respectively.

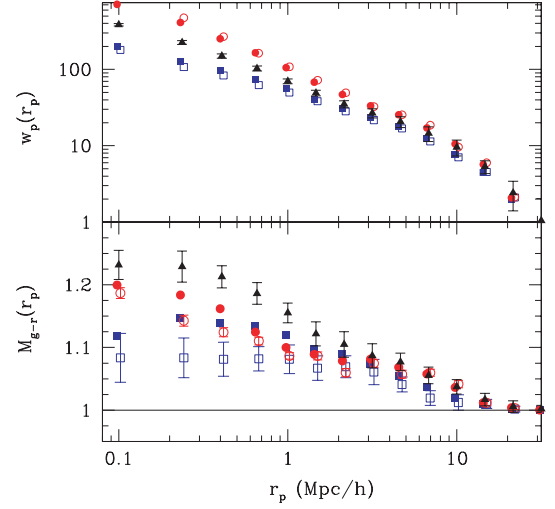


Figure A4. $g - r$ colour marked correlation function (lower panel) of all galaxies in the $M_r < -19.5$ catalogue (triangle points) compared to that of spiral and early-type galaxies (red circle points and blue square points), as in Fig. 7, but with the mark distributions forced to match the black dotted histogram in Fig. A3. Spiral and early-type subcatalogues are determined using the greater morphology likelihood as the distinguishing criterion (filled points) or using the likelihood threshold of $P > 0.8$ (open points).

early-type galaxies are more strongly clustered than red spirals, especially within the one-halo term. The apparent opposite trend in Fig. 7 was simply due to the extremely narrow colour distribution of early types (i.e. the colours were not allowed to depart significantly from the mean, so the colour marks of strongly clustered red early types were not much larger than the colour marks of bluer early types in less dense environments).

Finally, we compare the distribution of P_{el} , normalized by $P_{\text{el}} + P_{\text{sp}}$, to that of P_{red} in Fig. A5. The P_{red} distribution is more strongly peaked near 0 and 1 than that of P_{el} , simply because the colour distribution of galaxies is strongly bimodal, with an underpopulated

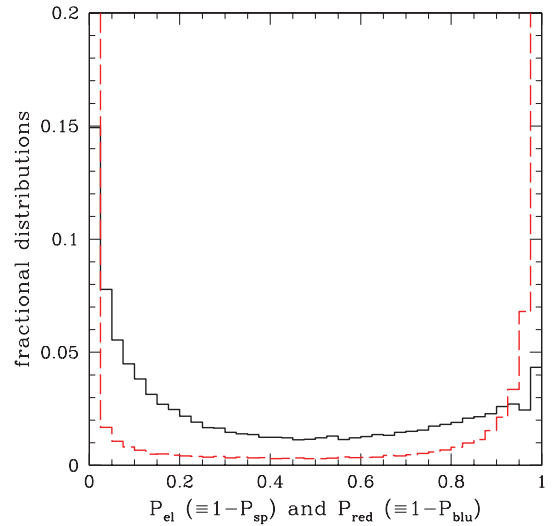


Figure A5. Distribution of P_{el} (solid black histogram), normalized so that $P_{\text{sp}} + P_{\text{el}} = 1$, and P_{red} (red dashed histogram), normalized so that $P_{\text{blu}} + P_{\text{red}} = 1$, in the $M_r < -19.5$ volume-limited catalogue.

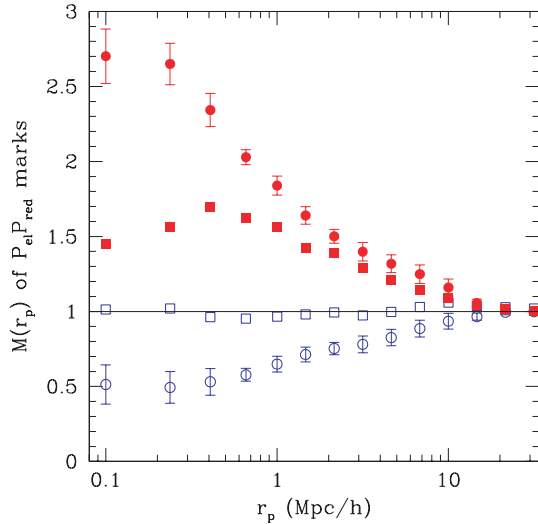


Figure A6. Marked correlation functions for the four colour–morphology combinations, $P_{\text{el}}P_{\text{red}}$ (red filled circles), $P_{\text{sp}}P_{\text{red}}$ (red filled squares), $P_{\text{el}}P_{\text{blu}}$ (blue open squares) and $P_{\text{sp}}P_{\text{blu}}$ (blue open circles), as in Fig. 9, but the distribution of P_{red} (and $1 - P_{\text{blu}}$) is forced to match that of P_{el} in Fig. A5.

‘green valley’, across much of the range of luminosities (Skibba & Sheth 2009).

Since the distribution of colour likelihoods is more strongly peaked at the minimum and maximum than the distribution of morphology likelihoods, it is possible that this could artificially strengthen the environmental dependence of colour vis-à-vis that of morphology. We account for this by maintaining the rank order of P_{red} of the galaxies in the catalogue, and giving them the same distribution as that of P_{el} . We then re-measured the marked correlation functions with the four colour–morphology combinations of P_{el} , P_{sp} , P_{red} and P_{blu} shown in Fig. 9. Fig. A6 shows the results, and they are almost the same. The only significant difference is that the $P_{\text{blu}}P_{\text{el}}$ mark appears to be uncorrelated with the environment at all scales, possibly due to the fact that blue early types are extremely rare (0.7 per cent). However, our conclusion that galaxies with high P_{red} and P_{sp} tend to reside in denser environments than average is robust.

This paper has been typeset from a $\text{\TeX}/\text{\LaTeX}$ file prepared by the author.